Modelling fatigue transition behaviour of FRP in mode I block loading

Master thesis report

L.J. Dupain

Delft University of Technology

TU Delft

Modelling fatigue transition behaviour of FRP in mode I block loading

by

L.J. Dupain

to obtain the degree of Master of Science
at the Delft University of Technology,
to be defended publicly on Friday May 12, 2023 at 14:15 PM.

Project duration:	November 2021 – May 2023	
Thesis committee:	Dr. ir. F.P. van der Meer	TU Delft, chair
	Dr. M. Pavlović	TU Delft
	Ir. P. Hofman	TU Delft, daily supervisor

TU Delft

Acknowledgement

This master thesis could not have been possible without my committee. First I would like to thank Frans van der Meer for giving the opportunity to do this thesis and sharing his insight on the topic. Where one can easily lose itself in the numerical methods, Marko Pavlocić encouraged me to keep the physical mechanisms in mind. It was refreshing to hear another perspective on the subject. I want to thank Pieter Hofman for his guidance and making the code of the model, including implicit fatigue damage update, available for me. During our weekly meetings the questions I had collected were patiently answered and we had some valuable discussions, which really helped me going. I would also like to express my gratitude for the flexibility and understanding of my committee when I had to pause my thesis for a while.
Lastly I want to thank Ruben for the technical support. The purpose was not always clear, but by asking the right questions and giving some explanation of the usage, we could resolve most problems.

L.J. Dupain
Delft, May 2023

Summary

According to experiments the fatigue damage behaviour of fibre reinforced polymers (FRP) experiences a load sequence effect. In this report the ability of the cohesive fatigue damage model of Dávila (2020) to simulate the behaviour after a load amplitude change is investigated. For this a double cantilever beam (DCB) with fictitious material properties is loaded in mode I. Two element layers with each its own cohesive law are used to take into account the different behaviour of the epoxy and the bridging fibres in the wake of the crack. The calculated crack growth rate is compared to the experiments done by Jensen et al. (2021b), since the conditions of the simulations are most similar to that of their experiments.

When the base and bridge layer only differ in their quasi-static cohesive law no load sequence effect is seen, since the conditions at the start of the second load block are the same as for the constant amplitude test at the same crack length. By allowing fatigue damage to accumulate only in the base layer and the bridge layer to only experience quasi-static loading, a history effect is seen. However, the high-to-low transition does not give the same transition behaviour as seen in experiments. In addition, the results of the constant amplitude tests are unrealistic.

When the fatigue damage accumulation of the bridge layer is faster than that of the base layer, a transition behaviour comparable, although less profound, to that of experiments is seen. This difference in fatigue damage accumulation is achieved by adjusting the coefficients of the fatigue damage rate function to the values corresponding to another R-ratio. This result may indicate a possible underlying mechanism for the transition behaviour of FRP.

Contents

1 Introduction

1.1. Background

Fibre reinforced polymers (FRP) consist of fibres, often glass fibres or carbon fibres, inside a resin. By adjusting for example the material of the fibres and resin the material properties of the FRP can be altered to fit the desired usage. An advantage of FRP is that they can have a large strength while being light weighted. Although the behaviour of FRP is investigated since the end of the twentieth century, a lot is still unknown. Especially the fatigue behaviour under variable amplitude is barely explored. Most of the experiments done to study the fatigue behaviour of FRP use constant amplitude tests and the models are aimed at predicting the residual lifetime and strength based on these constant amplitude loads.

In reality, however, structures are subject to load spectra, with variable amplitude and mode mixity. The damage propagation, and therefore the crack growth, depends on the damage already in the material and the current applied load. Some research (Jensen et al., 2021b) has shown that there is a load history effect when the mode I load exerted on a double cantilever beam (DCB) transitions from one block of constant amplitude to a block with another amplitude. Depending on whether the load amplitude transition is low-to-high or the opposite, an acceleration or retardation compared to constant amplitude tests is seen. The reason why FRP show this transition behaviour is still debated. A hypothesis is that the bridging fibres in the wake of the crack contribute to this history effect, but the exact contribution and how the bridging fibres work, is still researched. To be able to accurately predict the crack length and crack growth in FRP for realistic loading scenarios the transition behaviour should be incorporated in the model.

There are several types of fatigue models. Fatigue life models predict the fatigue life of the structure based mainly on stress-life curves (S-N curves). Post et al. (2008) compared several fatigue life models for variable amplitude loading. They distinguish damage accumulation based models, residual strength based models, micro-mechanics based models and fatigue modulus based models. A simple damage accumulation based model is Palmgren-Miner, also called Miner's rule:

$$D = \sum \frac{n_i}{N_i} \tag{1.1}$$

in which D is the damage, n_i is the number of cycles at stress level σ_i, and N_i is the number of cycles to failure at stress level σ_i. This model is independent of the load order. Variations of Miner's rule exist where the load sequence is taken into account. However, fatigue life models can not predict the crack growth and are therefore not suited for modelling the transition behaviour.

Progressive damage models do predict the evolution of the actual damage features, such as delamination. Pascoe et al. (2013) distinguish four classes: stress/strain based methods, fracture mechanics based methods, cohesive zone models (CZM) and extended finite element method (XFEM) based models. They note that "*stress/strain based methods are generally most applicable to static delamination problems, though there are a few uses of stress/strain methods in fatigue investigations in the literature.*" However, for fatigue applications stress/strain based models are only used to find a fatigue life

and do not predict delamination growth.
Fracture mechanics based models link fracture mechanics to the delamination growth, often by using a form of the Paris relation:

$$\frac{da}{dN} = C[f(G)]^m \tag{1.2}$$

in which a is the crack length, N is the number of cycles, $f(G)$ is a function of the the energy release rate G, and C and m are constants. By altering the function $f(G)$ certain effects, such as mode mixity and R-ratio dependency, can be incorporated in the model. Since the Paris relation only describes the crack propagation in the log-linear part, these types of models can not model the crack initiation and unstable crack growth. In finite element analyses the strain energy release rate (SERR) is often determined with the virtual crack closure technique (VCCT), which requires remeshing.
CZM contain cohesive zone elements at the interface along which delamination is expected. These elements have a prescribed traction-displacement relation, in which the type of softening can be specifically chosen based on the desired behaviour. By incorporating a damage parameter the stiffness of the element can be reduced, which simulates damage growth. CZM do not need remeshing and can include the initiation phase in the model. Six cohesive zone models are studied by Bak et al. (2017) on their capability to transition from quasi-static to fatigue loading. A promising model is the fatigue cohesive zone model of Dávila (2020). The model is capable of transitioning seamlessly from quasi-static damage to fatigue damage and vice versa. In contrast to the CZM of Turon et al. (2007) and the interfacial thick level set (ITLS) method of Latifi et al. (2017) the length of the fracture process zone l_c is not an input parameter, but calculated by the model. By superposing two bilinear cohesive laws, in which one layer represents the bridging fibres, the steady-state plateau in the R-curves can be simulated.
XFEM has enrichment functions to allow cracks to grow inside an element. By using cohesive laws inside a XFEM framework, delamination growth can be simulated.

1.2. Research objective

In this study the possibility of modelling the behaviour after a load amplitude change in a cohesive zone framework is explored. For simplicity this study is limited to a double cantilever beam (DCB) test in mode I block loading. The path of the crack inside a DCB is known a priori, therefore no XFEM framework is needed. For this study the fatigue damage model of Dávila (2020) is used. This model was choosen because of its capability to transition from quasi-static to fatigue damage and to calculate the fracture process zone length, in combination with the possibility to incorporate elements that represent the bridging fibres. This model is implemented in the Jem/Jive open source, research-oriented C++ programming toolkit from Dynaflow Research Group. The mesh is generated with Matlab and the post-processing is done with Python.

1.3. Structure of the report

This report starts with presenting a literature review in chapter 2. This chapter focuses on the fatigue behaviour, and especially the transition behaviour, seen in experiments. In chapter 3 the cohesive fatigue damage model used in this research is described, as well as the used geometry, load cases and material properties. The behaviour of the model and that of slightly adjusted models is discussed in chapter 4. This report closes with the main conclusions and recommendations for future research in chapter 5.

2

Literature study

In this chapter a literature study on the fatigue behaviour of FRP is given. First the failure mechanisms contributing to the fatigue behaviour are described. Next the behaviour after a load amplitude transition seen in experiments is summarised, and a phenomenological model capable of predicting the crack growth rate after a load amplitude change is reviewed.

2.1. Failure mechanisms

When FRP are delaminated, the surface in the crack wake is rough and there are fibres crossing over. The origin of these bridging fibres, as well as how bridging fibres can be incorporated in models, is reviewed in Khan (2019). They identified that bridging fibres can be formed due to for example a combination of a weak connection between the matrix and the fibres, and a large crack tip yielding zone. Ahead of the crack tip the strains increase, which eventually cause delamination or debonding of the fibres and the matrix. When this debonding takes place in a ply slightly above or below the crack tip, the delamination front will shift towards that layer and the fibres or bundles of fibres act as bridging fibres.

During crack propagation mechanisms like matrix cracking, fibre peeling, fibre-matrix pull-out and fibre tensile failure are active (Khan, 2019). These mechanisms interact with each other (Blanco et al., 2004), making the description of the crack propagation processes more complicated. Since the damage mechanisms and their interaction are not the same in quasi-static loading and cyclic loading, choosing an appropriate similitude parameter for modelling fatigue crack propagation should be done with care (Alderliesten, 2013).

For fatigue tests it appears that crack initiation is dominant at high stress levels and crack propagation at low stress levels, as it then has sufficient time to propagate (Bender et al., 2021 and Gamstedt and Sjögren, 2002). This statement is supported with the tests of Gamstedt and Sjögren (2002) on multi-directional laminates. They showed that the high-to-low block loading had a smaller lifetime than the low-to-high block loading due to the transverse cracks, viewed as an initiatory mechanism and formed during the high load block, being a starting point for the delamination during the low load block.

Fractographic analysis can indicate which mechanisms took place during the test. For a DCB loaded in mode I scanning electron microscopy (SEM) showed that fibre prints, which result form disbonding between fibres and matrix, and cusps, which form due to local shear stress between the fibres and matrix, are most dominant (Yao et al., 2015). For higher stress ratios more cusps are present. It was also noted that, independent of stress ratio, no significant plasticity was observed in the crack wake (Khan et al., 2014 and Yao et al., 2017).

A phenomenon seen in the delamination of FRP is the R-curve effect. This is the phenomenon of delamination toughness increasing with the crack extension until it reaches a steady-state value. This effect is seen for both quasi-static and cyclic loading (Yao et al., 2014a). Additional experiments (Yao et al., 2017) indicate that the R-curve effect is stress ratio dependent and that for a large R-ratio the R-curve is almost the same as for quasi-static loading. Bridging fibres are often seen as the cause for the R-curve effect, but mechanisms ahead of the crack tip may also play a role (Dávila et al., 2009).

The shielding effect due to the bridging fibres originate from the fibres taking up energy. As the crack opening displacement at the supports increases, the fibres are loaded and take up energy. In this process the effective applied energy at the crack tip is smaller, resulting in a decreasing crack growth rate. For cyclic loading, the bridging fibres periodically store and release energy during the loading and unloading phase respectively of cyclic loading (Yao et al., 2014b). Only when the fibres fail, the strain energy is permanently released. Eventually the bridging fibres are fully loaded and additional straining will result in bridging fibre failure due to tensile failure or fibre-matrix pull-out. At that point the steady-state value of the R-curve is reached.

Another shielding mechanism, besides fibre bridging, is crack closure. For a low stress ratio, the two faces of the crack can come in contact with each other during the unloading part of the load cycle. This contact can lead to compression. However, crack closure was only observed for some tests with a low stress ratios $0 < R < 0.17$ and even when it was present, the contribution to the decreasing crack growth rate was small (Khan et al., 2014), therefore the main focus is often on fibre bridging.

2.2. Behaviour after a load amplitude transition

The fatigue transition behaviour described in literature is not consistent. Some studies report a higher crack growth rate compared to the constant amplitude test after a load amplitude change, while others report a lower crack growth rate for the same transition. Sometimes this acceleration or retardation is seen directly after the load transition, but in other studies this response is delayed for several load cycles. It appears that the material and loading parameters are of great importance to the behaviour seen in experiments.

One of these loading parameters is the way the load is applied. The crack growth rate evolution is different for a DCB loaded in displacement control compared to load control, as shown by Stelzer et al. (2014). As the crack progresses, the specimen compliance increases. In displacement control this increased compliance causes a reduction of the effective applied load. Consequently the delamination rate decreases with increasing number of load cycles. Under load control the increasing compliance causes an increase in displacement and delamination rate. This makes load control more difficult with an increasing number of load cycles. Therefore, displacement control is often the preferred control mechanism for DCB tests.

Another important parameter is the configuration of the specimen. The loading conditions in joints are not exactly the same as in DCB tests. The crack growth of adhesively-bonded pultruded GFRP double-lab joints under block loading with load control is studied by Sarfaraz et al. (2013). For the low-to-high load amplitude transition the crack growth rate in the second block was higher than the corresponding constant amplitude test. The crack growth rate in the second load block after a high-to-low load amplitude transition was lower than that of the constant amplitude test. This retardation remained for a large number of load cycles until rapid failure. Their hypothesis for the crack growth acceleration and retardation is that different damage mechanisms are activated at different load levels. The acceleration after a low-to-high load transition could be caused by fibre breaking, while the retardation after a high-to-low load transition is due to a decreased input energy for crack propagation while the bridging fibres developed during of the previous load block stay the same.

The crack growth rate of an uni-directional DCB in mode I block loading with displacement control is studied by Jensen et al. (2021b). Compared to the crack growth rate of the constant amplitude tests, they found an acceleration for the low-to-high block loading and a retardation for the high-to-low block loading (figure 2.1). After the low-to-high load amplitude change the crack growth rate decreases and after approximately 10^5 cycles or 15 mm of crack extension the crack growth rate of the low-to-high block loading is the same as the high constant amplitude test. The crack growth rate after the high-to-low load amplitude change is at first the same as the low constant amplitude test. For a crack extension of approximately 10 mm the crack growth rate quickly decreases until it settles at a slower crack growth rate deceleration. Due to crack arrest and the high-to-low test being manually stopped, it is unclear if the crack growth rate of the constant amplitude test would be reached with continued cyclic loading. Their hypothesis for this acceleration and retardation is that during a higher load level more bridging fibres develop in the crack wake. Immediately after the low-to-high load transition, the fibre bridging zone is under-developed and therefore the resistance to crack growth is lower, causing a higher crack growth rate compared to the constant amplitude. As the crack progresses, the amount of bridging fibres in the crack wake gradually increase until it is the same as the high constant amplitude test and

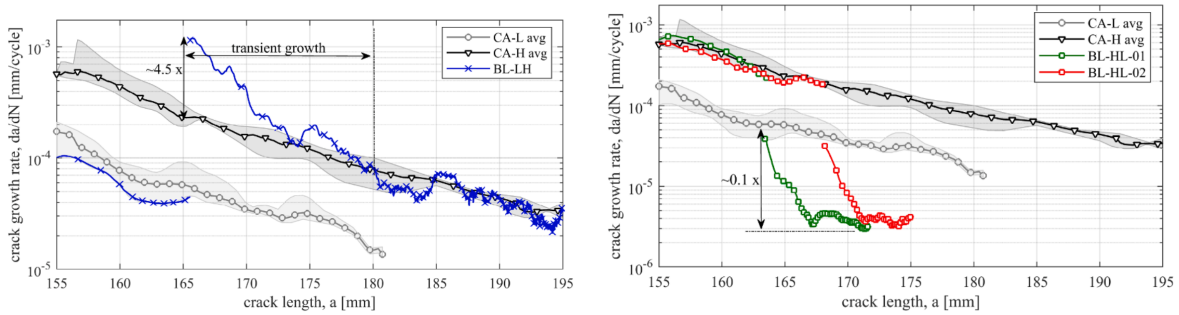

(a) Low-to-high block loading **(b)** High-to-low block loading

Figure 2.1: Crack growth rate and crack length for a DCB with displacement control, according to the experiments done by Jensen et al. (2021b)

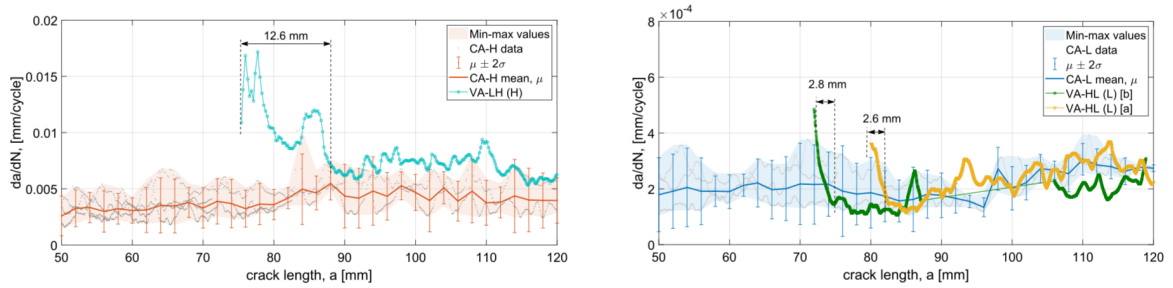

(a) Low-to-high block loading **(b)** High-to-low block loading

Figure 2.2: Crack growth rate and crack length during the second load block of a DCB with G-control, according to the experiments done by Jensen et al. (2021a)

consequently the crack growth rate is the same. The fibre bridging zone after the high-to-low load transition is over-developed compared to the constant amplitude test. The bridging fibres are partially unloaded and as they are gradually reloaded, the shielding effect increases, which causes the crack growth rate to decrease.

The SERR is often considered as the driving force for crack growth in fatigue. For a displacement controlled DCB test the SERR decreases during a constant amplitude test due to the increasing compliance with crack propagation. Although Jensen et al. (2021b) showed that for the same crack length and crack mouth opening displacement the SERR in each block of the block loading is the same as that of the constant amplitude tests, studying the crack growth rate after a load amplitude change for a G-controlled test, as is done by Jensen et al. (2021a), may give more insight. In a G-controlled test the SERR stays the same during the test. This can be achieved by applying a moment on the edges of the DCB. When the moments on the two arms are equal but have an opposite direction, mode I loading is obtained. Jensen et al. (2021a) found for both load amplitude transitions a higher crack growth rate compared to the constant amplitude tests (figure 2.2). The overshoot in crack growth rate decreases with continued cyclic loading and after a crack extension of 12.6 mm and 2.7 mm for the low-to-high and high-to-low transition respectively the crack growth rate is the same as the constant amplitude test. The transition behaviour of the high-to-low transition seen in the displacement control test and the G-control test is thus not the same.

2.3. Fatigue model with load amplitude transition

Some variations of Miner's rule exist in which the load sequence is taken into account. However, these models are damage based fatigue life models, which can not predict crack growth. To date, only one progressive damage model exist which takes the load sequence effects into account, namely the fracture mechanics based model of Jensen et al. (2023). In their model the crack growth rate is split into a steady-state (ss) term and a transient (tr) term:

$$\frac{da}{dN} = \frac{da}{dN}_{ss} + \frac{da}{dN}_{tr} \tag{2.1}$$

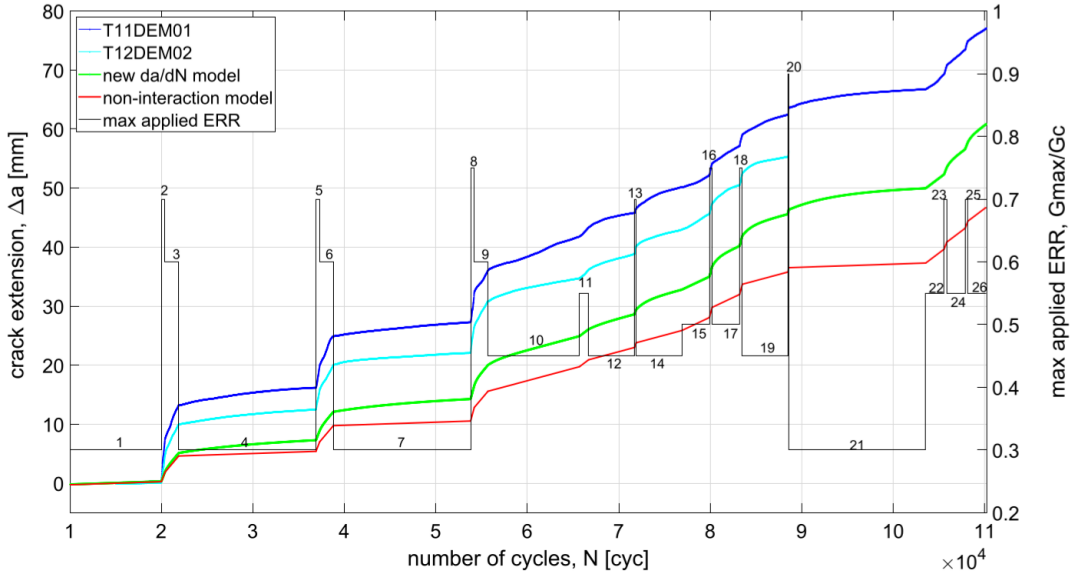

Figure 2.3: Crack extension of the G-control experiments (T11DEM01 and T12DEM02), a model with transient response and a model without transient response (adopted from Jensen et al., 2023)

The steady-state term is taken to be the Paris' law of the constant amplitude test. For the transient term an exponential decay function is used. The model parameters of the steady-state and transient functions are fitted to the results of a constant amplitude and block loading test in G-control respectively. These parameters are then generalised to be used for other load levels than the performed constant amplitude and block loading tests. According to their previous study on multiple block loading tests (Jensen et al., 2021a), "*the transient crack growth rate during consecutive H-load blocks is not necessarily a repeated response. A higher crack growth rate is observed in the initial H-load blocks in comparison to later H-blocks.*" The transient response in the low blocks on the other hand are independent of the number of previously experienced high load blocks. Since the transient response after a low-to-high transition depends on how much of these transitions has previously occurred, the model neglects this transient response and only takes the high-to-low transient response into account.

The resulting model is then used to simulate a multi-level block loading test, which is compared to a model without transient response and to the performed multi-level block loading experiment (figure 2.3). The new model predicts the crack growth rate after a high-to-low load amplitude change well. The error of the new model (-21.1%) is smaller than the error of the non-interaction model (-39.4%), but still the crack length is under estimated. The difference between the new model and the experiment mainly develops in the first few blocks of the test, since the low-to-high transient response is neglected while this transition, especially at the beginning of the test, cause a larger crack growth rate. Therefore the proposed model is not able to predict the crack extension accurately over the whole multi-level block loading test.

It should be noted that the model is only tested for a DCB in pure mode I loading with G-control and with a constant stress ratio $R = M_{min}/M_{max} = 0.2$. It is not known how the model performs for other loading conditions. Furthermore, the model does not offer any explanation on the underlying mechanisms for the transition behaviour seen in variable amplitude loading of FRP, as the model parameters are fitted to the constant amplitude and block loading experiments.

3 Method

This chapter describes the cohesive zone model used to simulate the transition behaviour. After a description of the model parameters, the values used in this study are given.

3.1. Model description

In this study the cohesive zone fatigue damage model of Dávila (2020), which is based on a S-N curve, is used. For the damage in an element it is assumed that the damage due to quasi-static loading and due to fatigue are a measure of the same physical state and can be accounted for by a single damage variable D. Although some studies (Yao et al., 2014a) indicate that the damage caused by quasi-static loading is not the same as the damage caused by load cycles, having a single damage parameter is convenient for simplicity.

During fatigue the damage accumulates while the stress is smaller than the strength σ_c of the material. The accumulating fatigue damage results in a reduction in stiffness. Since any point outside the cohesive envelope corresponds to a failed material state, the cohesive law is also the envelope of the damage process (Dávila, 2018). The fatigue damage is calculated with the fatigue damage rate function:

$$\frac{dD}{dN} = (D + \gamma) \left(\frac{\lambda}{\lambda^*} \right)^{\beta} \tag{3.1}$$

in which D is the damage norm, N is the number of cycles, λ is the displacement jump, λ^* is the reference displacement jump (figure 3.1), and β and γ are constants.
The damage norm, which can be interpreted as the ratio of the energy dissipated during the damage process over the critical energy release rate, and therefore also as the ratio of the damaged area over the area associated with the local discretisation, is defined as:

$$D = \frac{\lambda^* - \Delta_c}{\Delta_f - \Delta_c} \tag{3.2}$$

The coefficients β and γ are determined by fitting the number of cycles until failure N^F of an unnotched bar to the S-N curve. This N^F is calculated by integrating equation 3.1. The S-N curve is approximated by a straight line, with two anchor points. The first anchor point, which is at the end of the ductile range, is at two cycles. The second anchor point, which represents the endurance limit, is at 10^7 cycles. The endurance limit is calculated based on the Goodman diagram and the assumption that the endurance limit at R = -1 can be approximated with $\sigma_e = \sigma_c/3$. For more details on the determination of the coefficients β and γ, the reader is referred to Dávila (2020), in which it is stated that β and γ are material-independent coefficients. The β and γ for different R-ratios given in Dávila (2020) is used in this research. Other fatigue damage rate functions are studied in Dávila et al. (2020). However, in this research equation 3.1 is used due to its simplicity.

The cohesive zone model is based on the mixed-mode model of Turon et al. (2007) and can therefore take the dependence on the mode of fracture into account. This feature is not utilised in this research since it focuses on mode I loading.

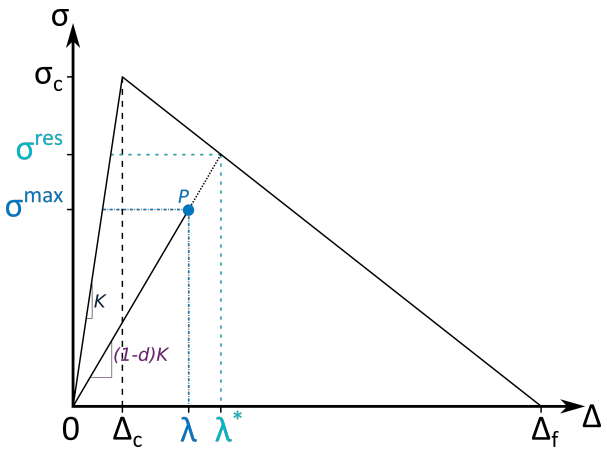

Figure 3.1: Cohesive law with fatigue damage and definition of displacement jump parameters (adopted from Dávila, 2020)

For high-cycle fatigue it is computationally inefficient to model the complete load cycles (Bak et al., 2017). Therefore the analysis is performed using simplified cyclic loading (SCL). In this procedure the maximum load is held constant and the number of applied cycles is pushed forward. The R-ratio incorporated in the coefficients β and γ takes into account the effect of the alternating load.

In contrast to the model described by Dávila (2020) the damage update of the integration points is done with an implicit method instead of an explicit method. The damage D of the previous step, the displacement jump λ and the cycle increment ΔN are the inputs for the trapezoidal method, which together with the fatigue damage rate function determines the damage of the integration points. If non convergence is found for the fatigue damage, the program gives a warning and continuous with the the nonlinear solver, even when the residual of the fatigue damage update is large.

For the analysis an adaptive stepping scheme is used. The cycle increment ΔN is increased based on the number of iterations needed to obtain equilibrium in the previous time step. An overview of the performed steps by the model is given in figure 3.2.

The used cohesive law determines which failure mechanisms are taken into account. For example, the R-curve effect in quasi-static loading can be modelled by using a bilinear softening law (Dávila et al., 2009, Heidari-Rarani et al., 2013 and Jensen et al., 2019). A relative simple way to obtain such trilinear cohesive law is by superposing two bilinear cohesive laws. In general one of these cohesive laws can be seen as the representation of quasi-brittle delamination fracture, which is characterised by a small displacement jump at failure, and the other as the effect of bridging fibres, characterised by a larger displacement jump at failure. However, Dávila et al. (2009) note that these "*two linear softening responses are used for convenience and do not necessarily correspond to two distinct failure modes which could peak at different displacement jumps.*"

In this study a bilinear softening law is used to account for the R-curve, as is done by Dávila (2020). For this two layers with each its own cohesive law are distinguished and superimposed. These layers share nodes and are named base and bridge, of which the last represents the bridging fibres present in the crack wake.

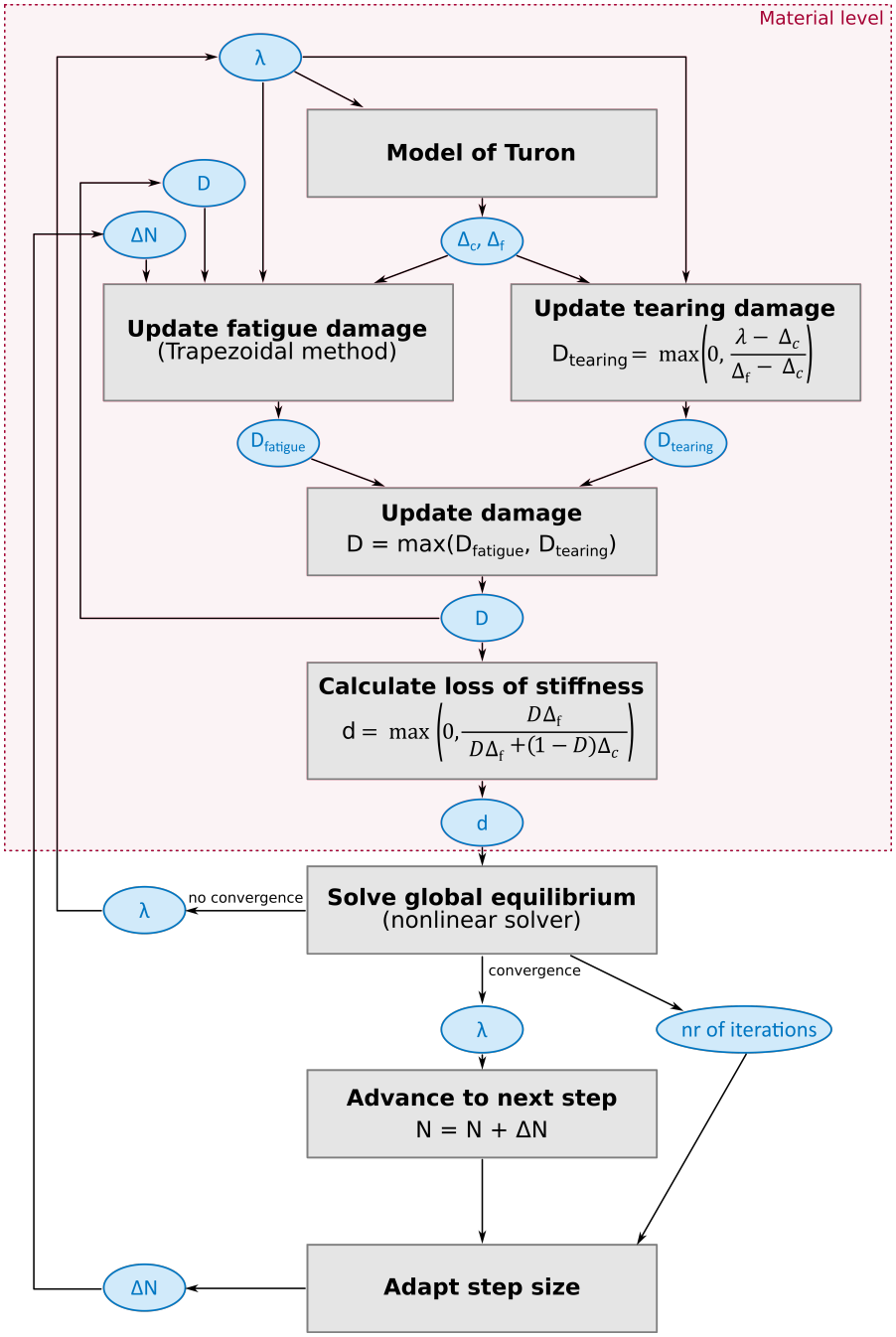

Figure 3.2: Overview of the analysis

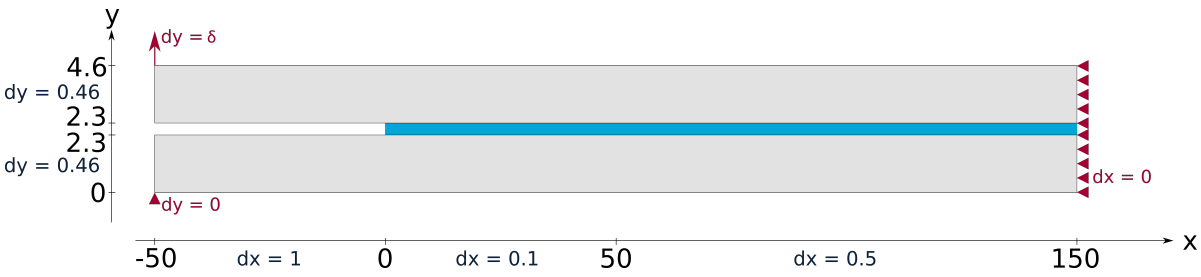

Figure 3.3: Mesh of the double cantilever beam including boundary conditions. The interface elements are shown in blue and the bulk material in grey.

Table 3.1: Dimensions of the double cantilever beam

Property	Symbol	Unit	Value
Length	l	mm	200
Height	$2h$	mm	4.6
Pre-crack length	a_0	mm	50

3.2. Input parameters

3.2.1. Geometry

The model as described in section 3.1 is tested on its ability to model the fatigue transition behaviour by simulating a DCB. For simplicity the DCB is modelled in 2D with plane strain conditions as opposed to 3D. Plane strain conditions correspond to a plane in the middle of the width of the beam.

The DCB has a length of 200 mm and plies of 2.3 mm thick. At the start of the simulation a pre-crack of 50 mm is present. The plies are modelled with 4-node rectangular elements with a height of 0.46 mm and 2 x 2 Gauss integration scheme. The interface between the plies is modelled with zero-thickness elements with linear shape function and a two point Newton-Cotes integration scheme.

Across the length of the beam the elements have different lengths (figure 3.3). The part of the interface closest to the pre-crack has elements with a length of 0.1 mm, since this is the region of interest. To speed up the calculation the element length in the pre-crack is 1 mm and at the end of the beam the element length is 0.5 mm.

At the right edge the horizontal displacement of the DCB is restrained and at the bottom left of the beam the vertical displacement is restrained. At the top left of the beam the load is enforced on the DCB in the form of a vertical displacement.

3.2.2. Load cases

The simulation is displacement controlled. The value of the imposed vertical displacement at the left top of the DCB and the number of cycles vary throughout the simulation. First the displacement is increased up to the value of the first load block. During the load block the displacement is kept constant and load cycles are imposed. If the test contains a second load block, the displacement is changed without enforcing cycles until the desired displacement is obtained, after which the load cycles of the second load block are applied. A schematisation of the applied load for the high-to-low block loading is shown in figure 3.4. The frequency of the cycles does not affect the simulation and thus the time is irrelevant.

Several load cases are distinguished (table 3.2). The first load case has fatigue cycles at a displacement before the maximum load bearing capacity of the DCB. At the start of these cyclic loading load blocks the bridging fibres in the crack wake are not fully developed. For the other load cases, with a displacement after the maximum load bearing capacity of the DCB, the cohesive zone is fully developed. The number of cycles of load case 1 and 2 are chosen such that during the transition from a low to a high load block a quasi-static response is avoided (figure 3.5). During the transition from a low to a high load block for load case 3 the response of the DCB follows the quasi-static response,

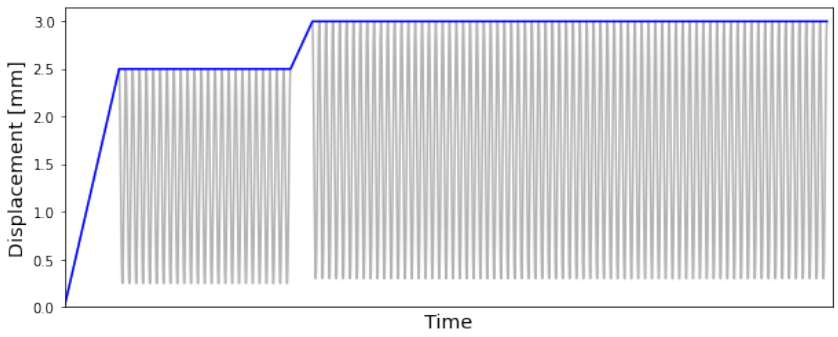

Figure 3.4: Schematization of displacement throughout a low-to-high block loading test. The blue line represents the load used in the model.

Table 3.2: Characteristics of the load cases. δ^L_{max} and δ^H_{max} are the displacement during a low and high load block respectively.

Load case	Cohesive zone	δ^L_{max} [mm]	δ^H_{max} [mm]	During transition low-to-high
1	Not fully developed	2.5	3.0	No quasi-static response
2	Fully developed	6.5	7.0	No quasi-static response
3	Fully developed	6.5	8.0	Partly follows quasi-static response

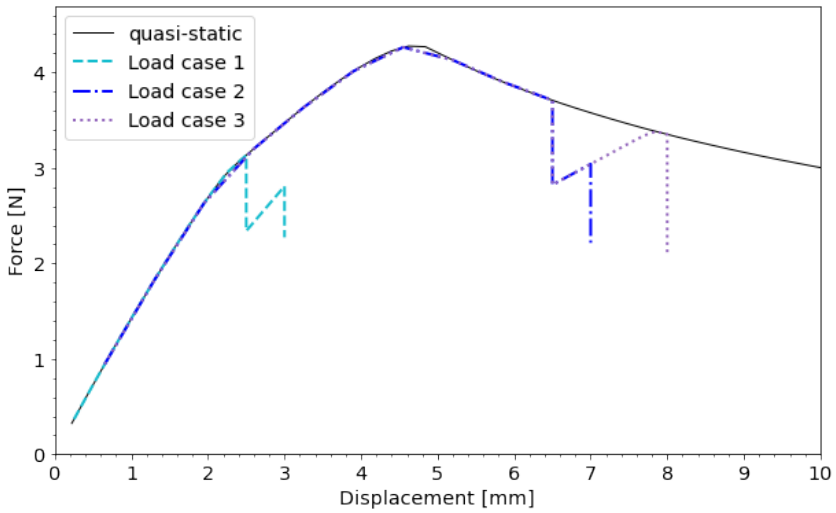

Figure 3.5: Applied displacement and reaction force at the top left support for the quasi-static and the low-to-high block loading test for several load cases

since the displacement of the high load block of load case 3 is larger than that of load case 2, while the displacement of the low load block and the number of cycles are the same. For all load cases the number of cycles of the low load block after the high load block is chosen such the fatigue damage increases. The number of cycles of each test and for all load cases can be found in appendix A. The ratio between the minimum and maximum displacement inside a load block is $R = \delta_{min}/\delta_{max} = 0.1$ for all load cases.

In this report the constant amplitude tests are denoted as ca_L and ca_H, in which the L and H indicate a low and high amplitude respectively. The low-to-high block loading test is denoted as va_LH and the high-to-low block loading as va_HL.

3.2.3. Material properties

It is expected that the bridging fibres play an important role in the transition behaviour. To be able to investigate the effect of the bridging fibres, a fictitious material with dominant bridging elements is used in the performed simulations. The tensile strength f_t and stiffness k of the base and bridge layer are chosen such that the superposition of the cohesive law of the layers is trilinear, as shown in figure 3.6. Although FRP are orthotropic, the plies are assumed to be isotropic by using Hooke's law, because the focus of this study is on the cohesive interface elements. The material properties of the fictitious material are summarised in tables 3.3 and 3.4.

3.2.4. Solver parameters

For the analysis a nonlinear solver is used with a tolerance of 1.0e-5 and a maximum of 25 iterations. The trapezoidal method to update the fatigue damage at material level has a tolerance of 1.0e-10 and a maximum of 100 iterations.

Table 3.3: Material properties of the interface

Property	Symbol	Unit	Base layer	Bridge layer
Tensile strength	f_t	N/mm²	15.0	3.0
Fracture energy mode I	G_{Ic}	Nmm/mm²	0.15	0.375
Dummy stiffness	k	N/mm³	1.0e5	2.0e4
Shear strength	τ	N/mm²	30.0	30.0
Fracture energy mode II	G_{IIc}	Nmm/mm²	1.0	1.0
Mode mixity	η	-	5.0	5.0

Table 3.4: Material properties of the plies

Property	Symbol	Unit	Value
Young's modulus	E	N/mm²	115e3
Poisson ratio	ν	-	0.3

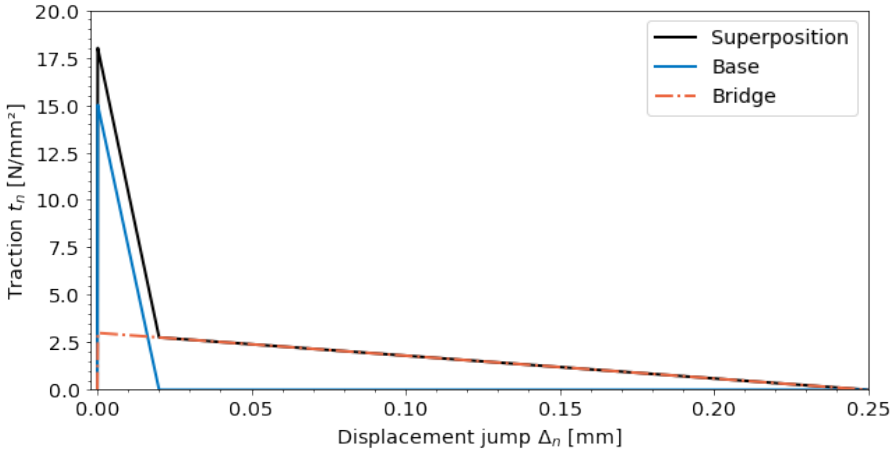

Figure 3.6: Cohesive law of the base and bridge layer of the fictitious material

4

Results

The model as described in chapter 3 is tested on its ability to model the fatigue transition behaviour by simulating a double cantilever beam test. The results of the performed tests are presented in this chapter. First the calculation of the crack length is given, since this definition is used for all simulations. The results of the simulation of a material without bridging layer is discussed for completion, after which the results of the model with bridge layer is shown. Small adjustments are made with respect to the damage accumulation in the cohesive elements and the effect of these adjustments are discussed. Since the conditions of the simulations are most similar to the experiments by Jensen et al. (2021b), the results are compared to the transition behaviour seen in those experiments.

In cohesive zone models the crack tip is often defined as the first point that can not sustain cohesive tractions and is thus fully damaged. The physical crack tip is at the point where delamination initiates, which is around the point with maximum traction. The cohesive zone, in which the damage develops, is between the physical crack tip and the fully damaged elements.
The location of the crack tip is determined based on the data of the base layer only, since the base layer represents the epoxy. The crack length is calculated with:

$$a = a_0 + \sum_{e=0}^{n} D_e l_e \tag{4.1}$$

in which a is the crack length, a_0 is the pre-crack length, e is the element number, n is the total number of elements in the interface, D_e is the damage of the left integration point of the base layer and l_e is the element length. Other definitions of the crack length, for example taking the point of maximum traction, changes the value of the calculated crack length and may result in less smooth graphs, but the overall trend of the crack growth is the same.

4.1. Model without bridge layer

The total fracture energy G_{Ic} of the model with only the base layer is smaller than the model with a bridge layer. Consequently the maximum load bearing capacity of the DCB is smaller. The displacement of the load cases is adjusted such that load case 1 is before and load case 2 is after the peak load.

The tractions along the interface of the DCB are shown in figures 4.1 and 4.2. In contrast of load case 2, the traction at the initial crack tip is nonzero after the load transition for load case 1. This indicates that the cohesive zone is not fully developed for load case 1. During the second load block of the low-to-high test of load case 1 the traction at the initial crack tip becomes zero. At that time the accumulated damage results in such a stiffness reduction that the corresponding quasi-static response, obtained by quasi-statically loading the DCB until the quasi-static response, experiences softening and the cohesive zone is fully developed.

During the cyclic loading the crack progresses and the traction profile moves accordingly. When the cohesive zone is fully developed, the crack progresses while the tractions maintain their general shape. This profile is also noticeable when the cohesive zone is not fully developed, only to be cut off

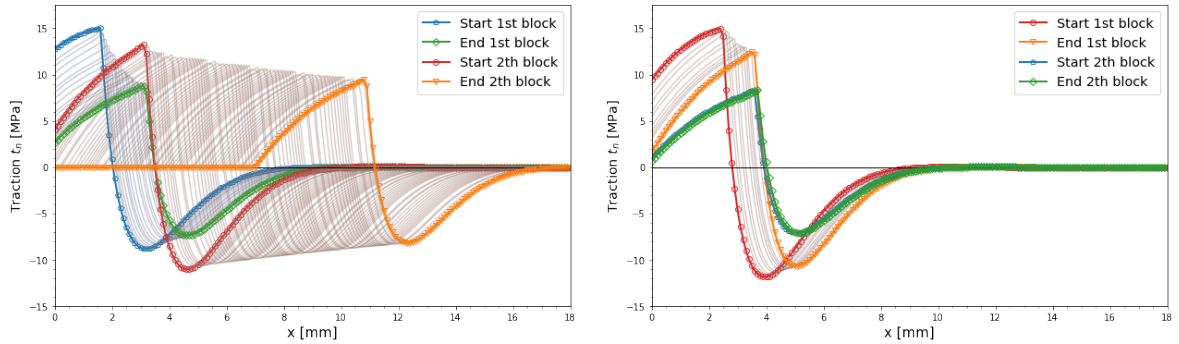

(a) Low-to-high block loading

(b) High-to-low block loading

Figure 4.1: Traction along the interface during the two load blocks for load case 1

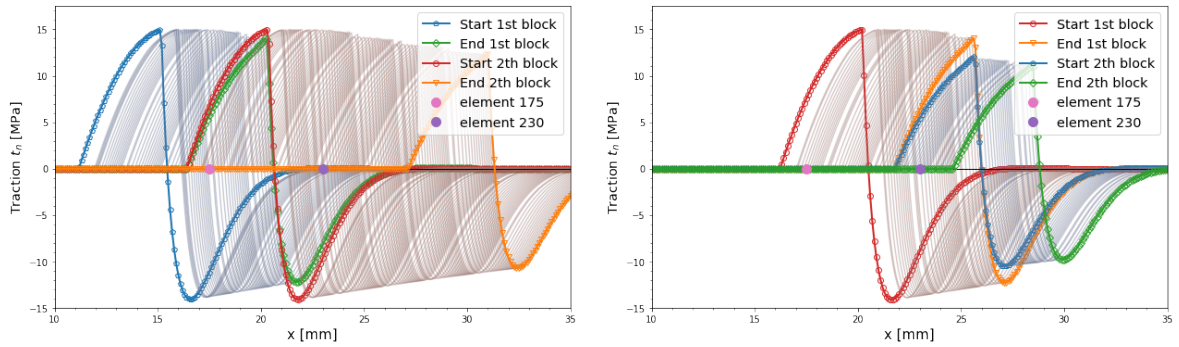

(a) Low-to-high block loading

(b) High-to-low block loading

Figure 4.2: Traction along the interface during the two load blocks for load case 2

at the initial crack tip. As the crack progresses, the stiffness reduces while the applied displacement stays the same. The dissipated energy and the magnitude of the tractions therefore decreases during a load block.

When fatigue cycles are applied the integration points of the elements leave the cohesive envelope to a state inside it. After a certain settling length, the integration points follow a path parallel to the cohesive law. In figure 4.3 the path inside the cohesive envelope throughout the simulation is visualised for one single integration point. The path during the constant amplitude tests and a block loading test are shown. At the load transition the integration point experiences secant loading or unloading for va_LH and va_HL respectively, after which it follows the path of the constant amplitude test. This secant loading and unloading represents a transition without damage accumulation. Only when the quasi-static response is followed during the low-to-high transition, as for load case 3, damage accumulation takes place. For that transition the tractions first increase without damage accumulation until the integration points reach the cohesive envelope and follow it.

For each time step the crack growth rate da/dN is calculated and plotted against the crack length a. During the load transition the applied cycles dN is zero and consequently the crack growth rate da/dN reaches infinity. Since these values are unrealistic, they are filtered out.

In figure 4.4 the crack growth rate of the block loading simulations is compared to that of the constant amplitude simulations. The geometry and material properties are the same, only the applied load is different. Both the high-to-low and the low-to-high transition are piece-wise coincident with the constant amplitude curves. This behaviour is seen for both load case 1 and load case 2, which indicates that the cohesive zone development does not influence the crack growth behaviour.

The piece-wise coinciding crack growth rate curves indicate that the crack growth is independent of the load history and follows Miner's rule. However, as explained in chapter 2, experiments indicate that FRP experience a load sequence effect. The behaviour of the model differs from the behaviour observed in experiments.

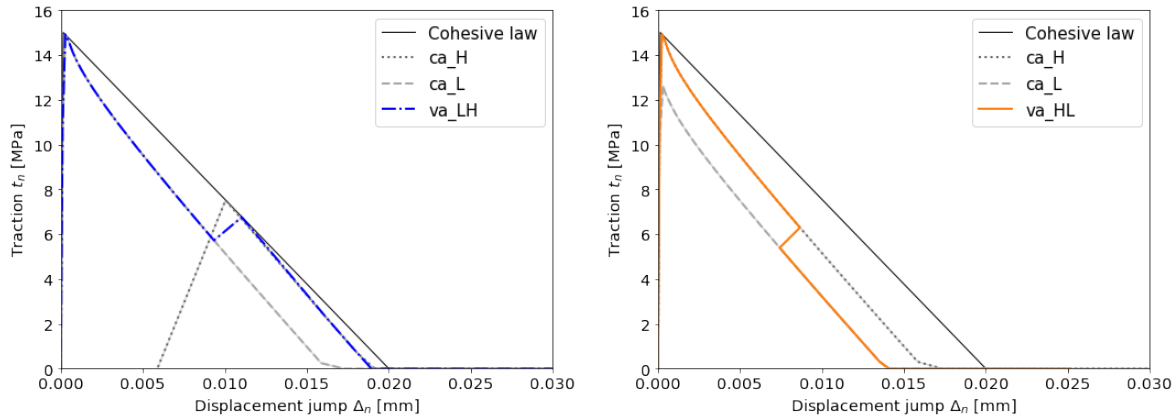

(a) Element 175 of the low-to-high block loading

(b) Element 230 of the high-to-low block loading

Figure 4.3: Traction and displacement jump of the left integration point of an element for all time steps for load case 2 of the model without bridge layer

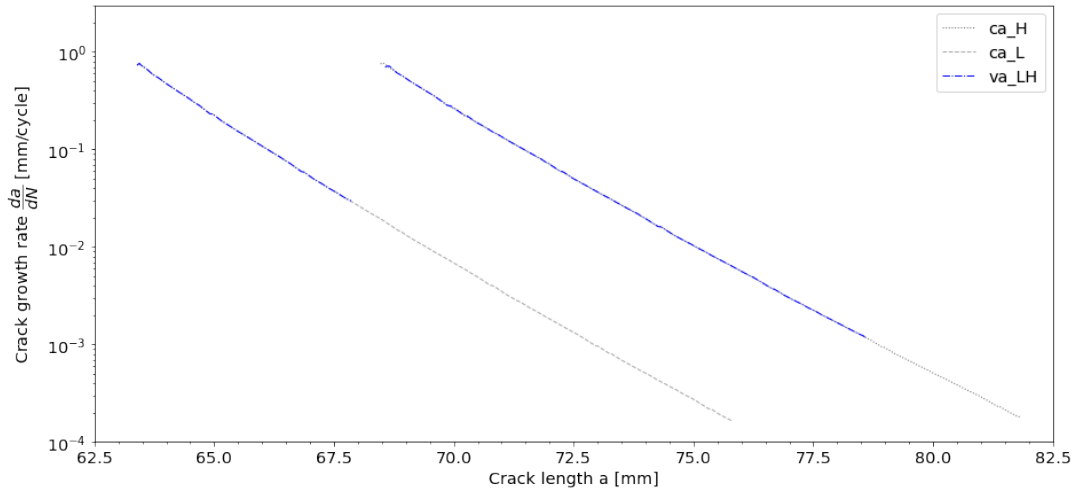

(a) Low-to-high block loading

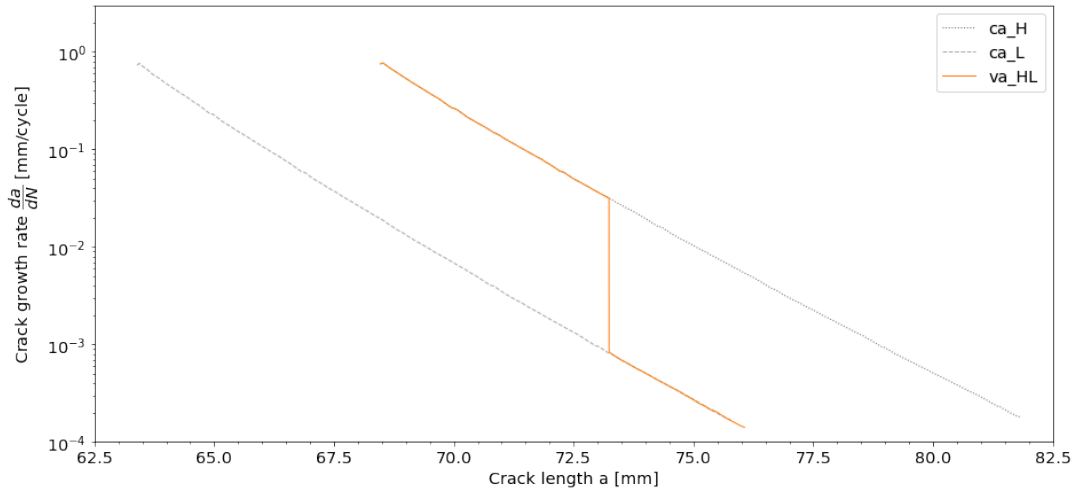

(b) High-to-low block loading

Figure 4.4: Crack growth rate and crack length of load case 2 of the model without bridge layer

4.2. Model with bridge layer

By using a base and bridge layer more failure mechanisms are incorporated, which makes the model more realistic. The sum of the tractions of the base and bridge layer along the interface of the DCB are shown in figure 4.5, alongside the deformation of the interface. In the crack wake two zones can be distinguished: a part where both the base and bridge layer have nonzero tractions, and a part where the base layer elements are fully damaged while the bridge layer has nonzero tractions. The relative large displacement jump at failure of the bridge layer causes a longer cohesive zone than the model without bridging. At the start of the first load block of load case 1, the traction at the initial crack tip is nonzero, indicating that the cohesive zone is not fully developed. It should be noted that at that time step the traction of the base layer at the initial crack tip is zero. When the applied displacement is in the global softening behaviour, as for load case 2, the cohesive zone is completely formed at the start of the first load block.

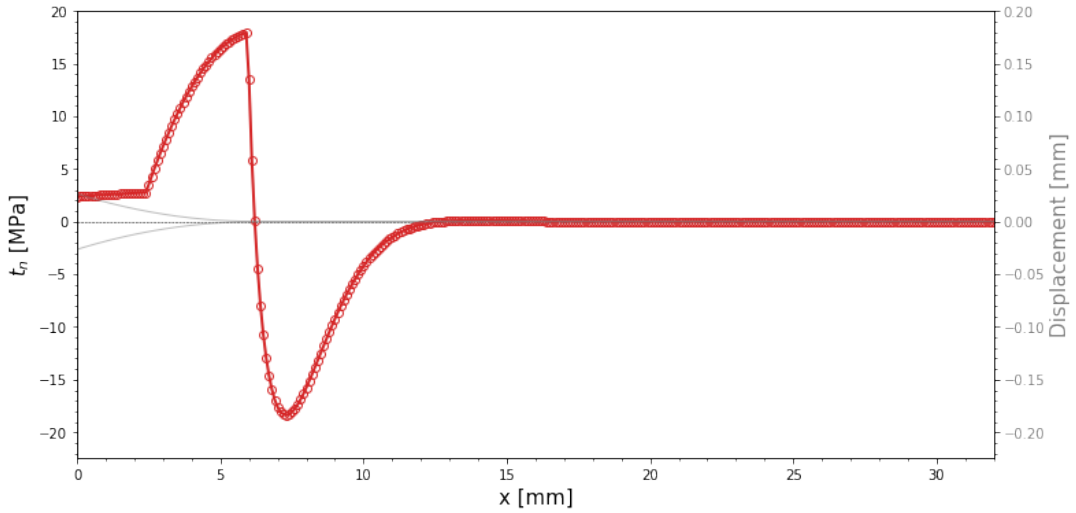

(a) Load case 1

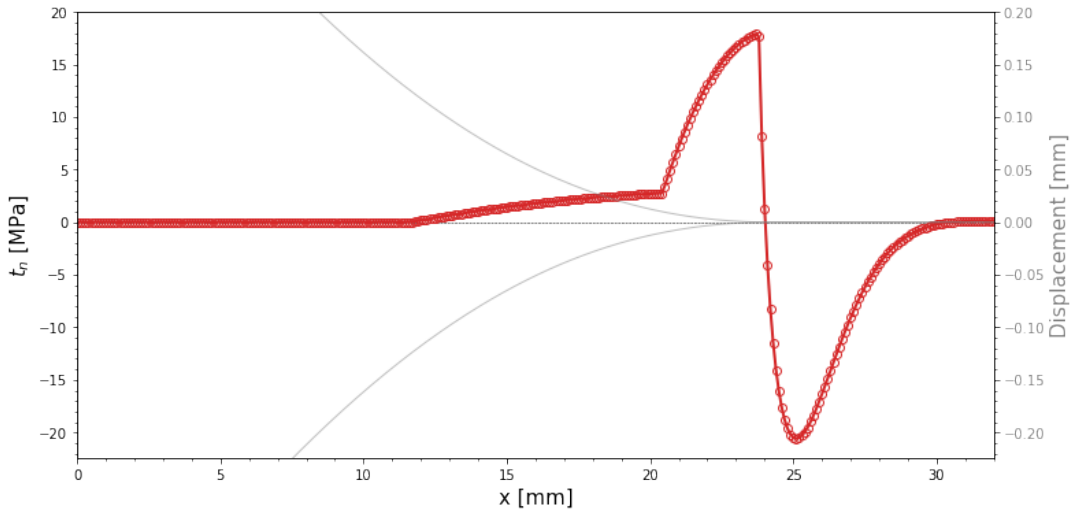

(b) Load case 2

Figure 4.5: Sum of the traction of the base and bridge layer and deformation along the interface at the start of the first load block for va_HL of the model with bridge layer

The crack progresses similar to the model without a bridge layer. The shape of the tractions along the interface stays the same as the crack grows, while the magnitude of the tractions decrease. This reduction in dissipated energy as the crack progresses becomes also clear when for each time step the tractions of all elements are plotted against the corresponding displacement jump (figure 4.6). The lines in that figure correspond to a certain time step. Since the base and bridge layer only differ in

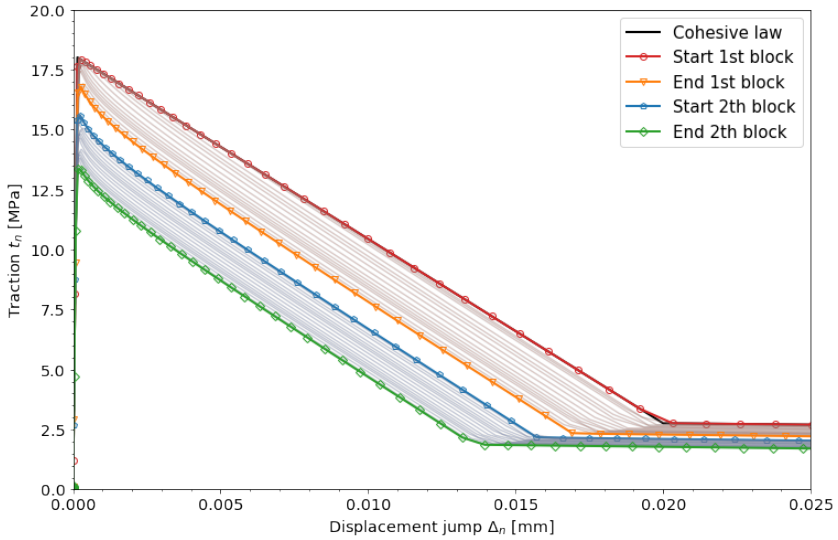

Figure 4.6: Sum of the traction of the base and bridge layer and displacement jump of all elements during the two load blocks of va_HL of load case 2 for the model with bridge layer

tensile strength and fracture energy, and consequently the displacement jump at failure Δ_f, the base and bridge layer work in a similar way. Just as in the base layer, the integration points in the bridge layer follow a path inside the cohesive envelope during fatigue loading. At the load transition the integration points experience secant loading or unloading, just as for the model without bridge layer. This secant loading and unloading takes place in both the base and bridge layer, thus when they are superimposed the secant loading and unloading holds. After the load transition the integration points follow the path of the constant amplitude test of the second load block.

In figure 4.7 the crack growth rate da/dN of the block loading tests is compared to the constant amplitude tests. Both load transitions are piece-wice coincident with the constant amplitude curves, which differs from the behaviour seen in experiments. Note that the crack length is calculated based on the damage in the base layer and that the damage in the bridge layer is not taken into account. When the crack length is calculated based on both the damage in the base and bridge layer, the calculated crack length differs, but the crack growth rate should be the same due to the tractions preserving its shape during crack propagation.

The model as described in chapter 3 does not model the desired transition behaviour. Experiments indicate a crack growth acceleration for the low-to-high transition and a retardation for the high-to-low transition, while the model shows a behaviour independent of the load history, as can be seen in figure 4.7. At the start of the second load block, the location of the integration points in the cohesive envelope is the same as the constant amplitude test at that crack length.

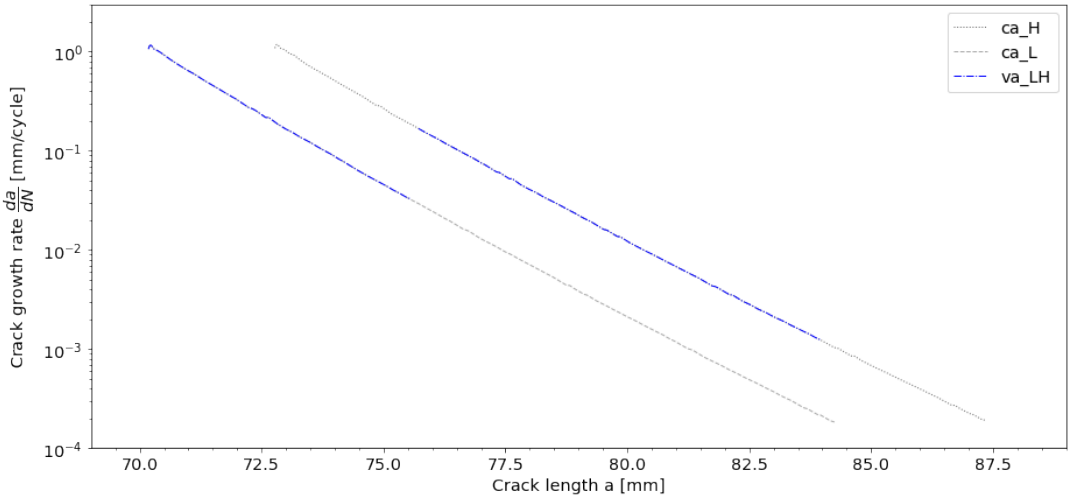

(a) Low-to-high block loading

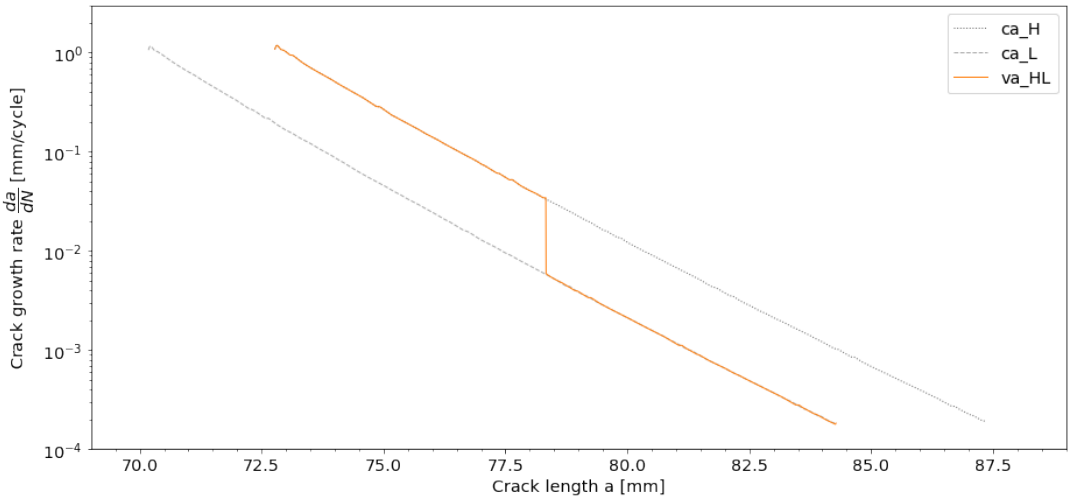

(b) High-to-low block loading

Figure 4.7: Crack growth rate and crack length of load case 2 of the model with bridge layer

4.3. Effect of no fatigue damage in the bridge layer

To be able to see a difference in response due to a history effect, the state of the DCB at the start of the second load block should not be exactly the same as the constant amplitude test at that crack length. The displacement at the support will always be the same, since it is a displacement controlled test. Furthermore the tests are compared at the same crack length, which is determined based on the base layer, so the SERR at the crack tip is the same. A difference will originate from the bridge layer. When for example the cohesive zone length of the bridge layer differs, the stress distribution and the shape of the plies in the cracked part will be different. Another possibility to have different conditions is when the integration points have a different position in the cohesive envelope. This means that at the same displacement jump, the tractions and damage are different.

For the original model, as described in section 3.1, the location of the integration points in the cohesive envelope is the same for the beginning of the second load block and the constant amplitude test. A way to have different conditions at the start of the second load block is by allowing fatigue damage only to develop in the base layer and not in the bridge layer. The integration points of the bridge layer follow the quasi-static cohesive law and can only enter the cohesive envelope during unloading. This adjustment represents the difference in loading of the epoxy and the bridging fibres. The exact behaviour of the bridging fibres and their damage accumulation during fatigue loading is unknown. It might be possible that during a DCB test the bridging fibres do not experience fatigue damage, but only fail due to tearing.

In figure 4.8 the crack growth rate of the constant amplitude tests for the model in which the bridge layer does experience fatigue damage is compared to that of the model without fatigue damage in the bridge layer. At the same crack length and for the same amplitude, the crack growth rate of the model without fatigue damage is lower than for the model with fatigue damage. This difference may originate from the dissipated energy needed for crack propagation. The integration points of the bridge elements of the model without fatigue damage can only follow the cohesive envelope during crack propagation. Therefore the energy needed for crack propagation is larger than for the model with fatigue damage in the bridge layer.

For the model with fatigue damage in the bridge layer the crack growth rate follows a straight line on log-scale, while the crack growth rate of the model without fatigue damage in the bridge layer follows a curved line. This indicates that the the underlying failure mechanisms simulated by the models differ from each other. The straight line of the model with fatigue damage is more in line with the trend seen in the experiments done by Jensen et al. (2021b). For both models the curves are approximately parallel for different constant amplitude tests.

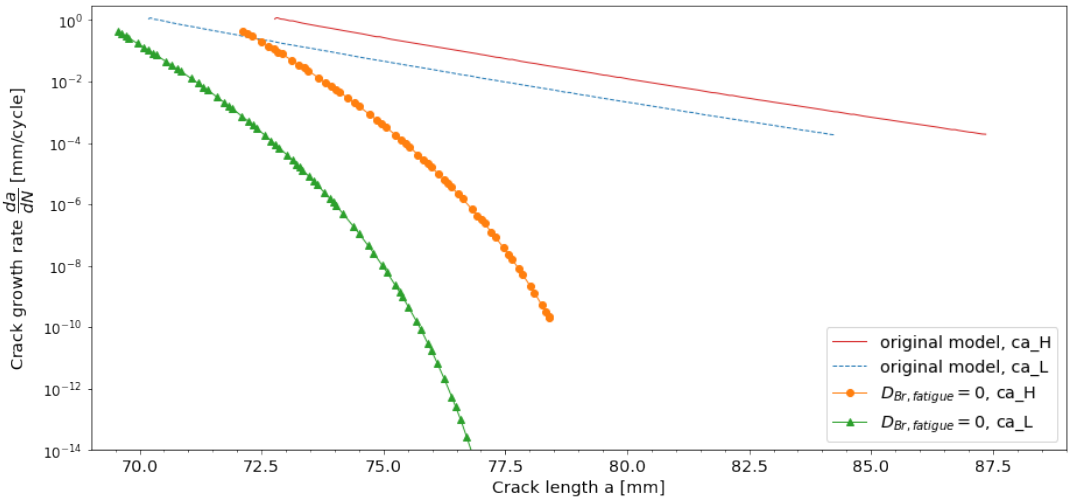

Figure 4.8: Crack growth rate and crack length of load case 2 for the original model with bridge layer and the model without fatigue damage in the bridge layer

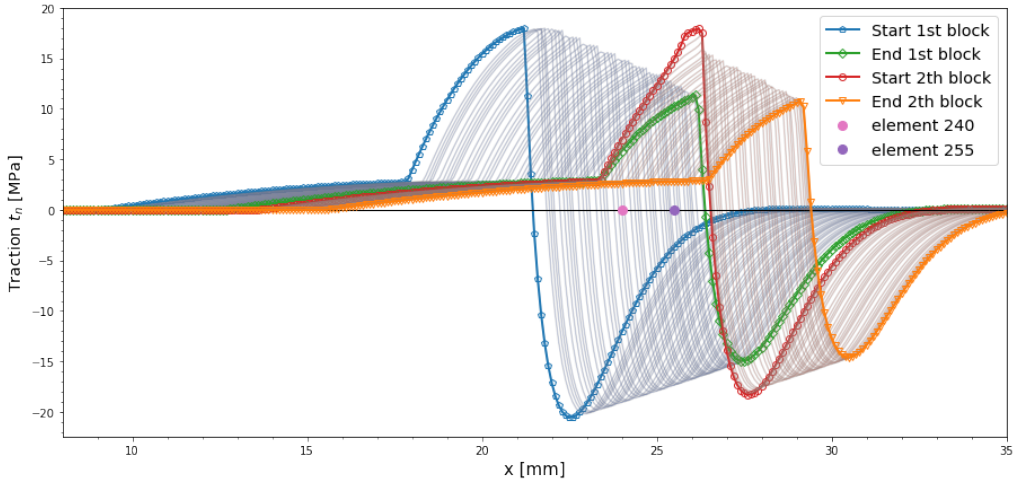

(a) Low-to-high block loading

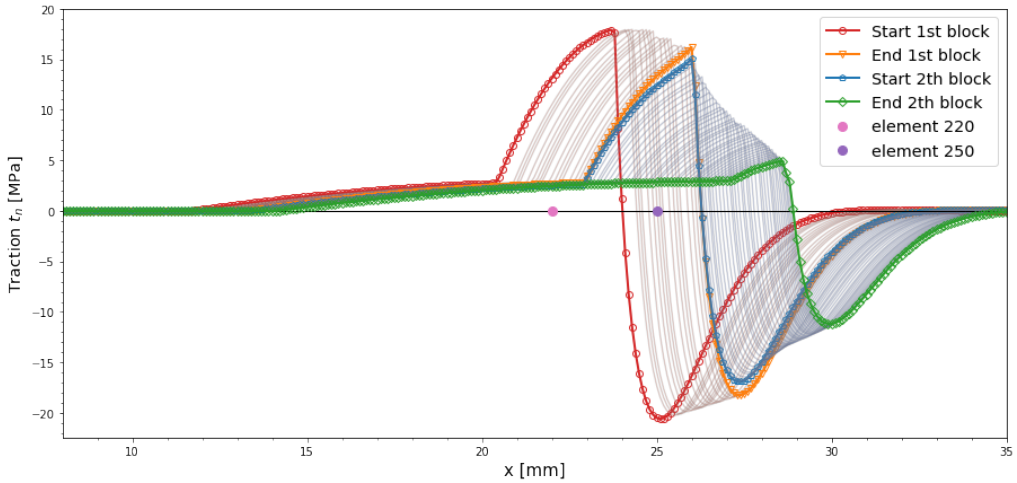

(b) High-to-low block loading

Figure 4.9: Sum of the traction of the base and bridge layer along the interface during the two load blocks for load case 2 for the model without fatigue damage in the bridge layer

During the first load block the development of the tractions are similar for both the model with and without fatigue damage in the bridge layer. The magnitude of the tractions decrease, while the shape of the traction profile stays approximately the same. This shape changes during the low-to-high transition (figure 4.9a).

In the base layer the traction of all elements grow during the low-to-high transition. The elements in the crack wake at maximum 0.5 mm from the crack tip experience tearing (figure 4.10a) during the transition to the high load block and the crack progresses slightly. Further in the crack wake no base elements become more damaged. During the transition to the high load block the integration points get a larger displacement jump and thus the tractions in the crack wake decrease. At the end of the crack wake some bridge elements become fully damaged, which represents the breaking of bridge fibres.

At the start of the second load block the base elements near the crack tip become more damaged while further in the crack wake the damage of the elements stays the same. Since the crack length is determined based on the damage in the base layer, the calculated crack length increases. The traction near the crack tip decrease until the traction profile shape is regained. This shape then progresses with the same crack growth rate as the high constant amplitude test.

The path inside the cohesive law of a single integration point throughout the block loading simulation is compared to the constant amplitude simulations in figure 4.11. During the load transition the base elements experience secant loading, which for the combined elements is visible as secant loading with the tensile strength of the bridge elements as origin. At the start of the second load block, the

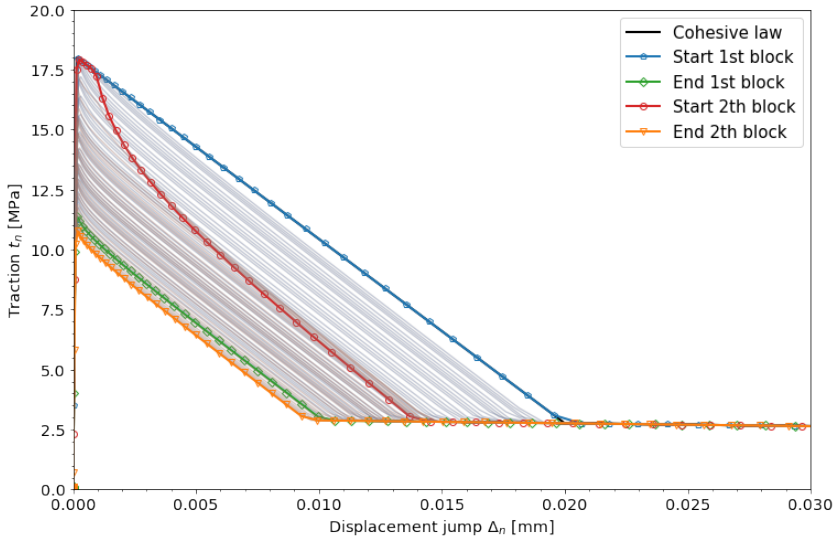

(a) Low-to-high block loading

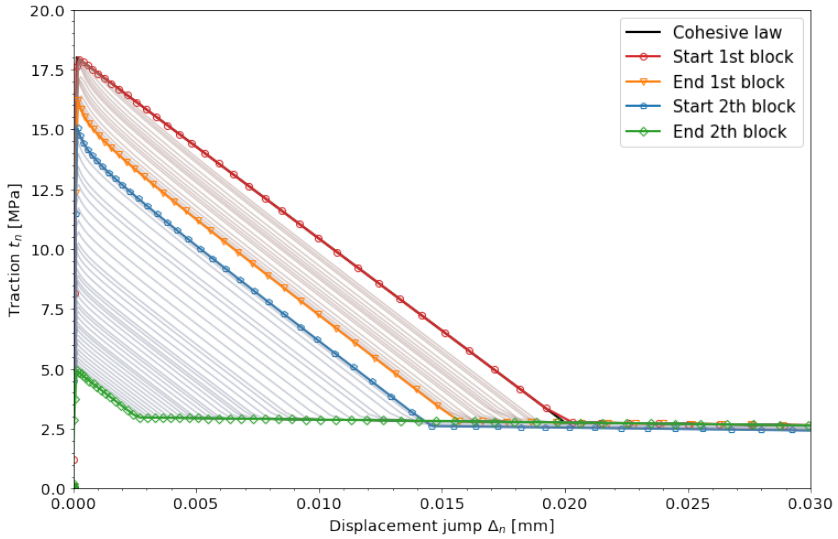

(b) High-to-low block loading

Figure 4.10: Sum of the traction of the base and bridge layer and displacement jump of all elements during the load blocks of load case 2 for the model without fatigue damage in the bridge layer

elements further away from the crack tip have a slightly lower traction than the constant amplitude simulation (figure 4.11a), while elements closer to the crack tip have a larger traction (figure 4.11b). The transition between lower and higher traction compared to high constant amplitude test is around element 244. During the second load block the integration points gradually move to the path of high constant amplitude test.

On global level, a small acceleration compared to the constant amplitude test is seen for the low-to-high block loading test (figure 4.13a). After 85 cycles and a crack extension of approximately 0.15 mm the block loading test experiences the same crack growth rate as the constant amplitude test. During these 85 cycles the shape of the tractions is regained. The transition behaviour seen for load case 1 is the same as for load case 2, which indicates that the cohesive zone development does not influence the results. The quasi-static crack propagation during the load transition of load case 3 is such that no load transition effect is seen during the second load block. The acceleration after a low-to-high load amplitude transition seen in experiments is larger and for more load cycles. However, having no fatigue damage in the bridge layer does give the same trend.

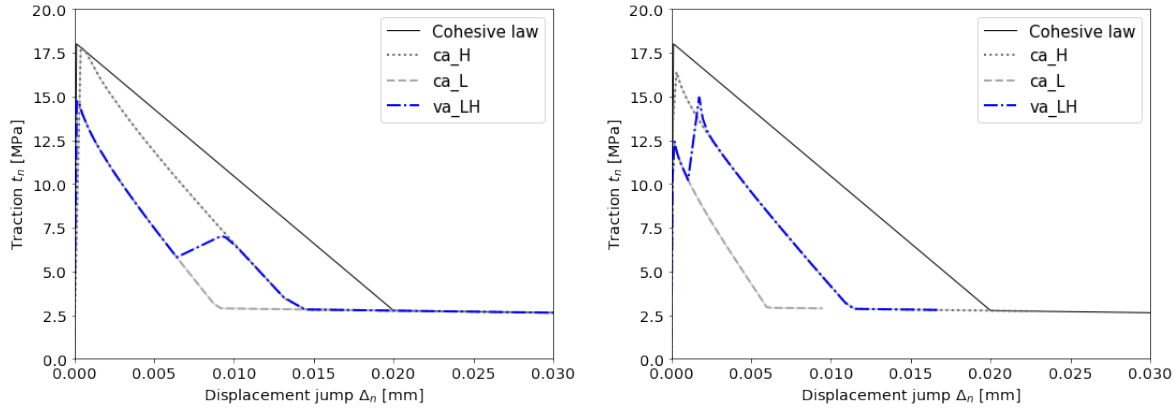

(a) Element 240 **(b)** Element 255

Figure 4.11: Sum of the traction of the base and bridge layer for the low-to-high block loading of load case 2 for the model without fatigue damage in the bridge layer

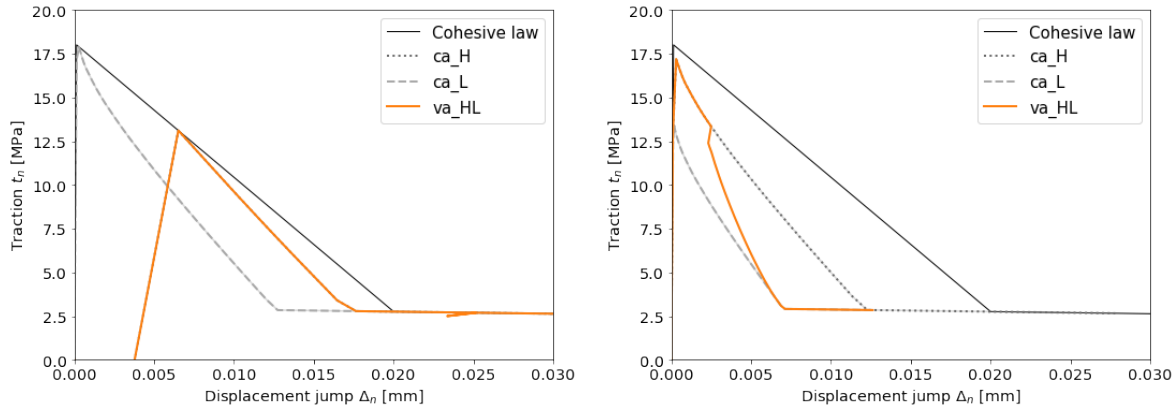

(a) Element 220 **(b)** Element 250

Figure 4.12: Sum of the traction of the base and bridge layer for the high-to-low block loading of load case 2 for the model without fatigue damage in the bridge layer

During the transition from the high to the low load block the displacement of the elements becomes smaller and the integration points experience secant unloading. The first approximately $2.5\text{e}9$ cycles of the second load block the damage in the bridge elements increases fromout the crack tip. The bridge elements around the crack tip are reloaded first. When the bridge elements at the end of the crack wake are reloaded, the elements at the crack tip have developed more damage and moved along the cohesive envelope. The more damaged elements have a smaller traction, therefore elements right of the crack tip must take up some traction to maintain equilibrium. In this process the crack front propagates. The tractions in the base layer move, while maintaining its general shape, accordingly with this propagating crack front. After approximately $2.5\text{e}9$ cycles all elements are reloaded and the whole traction profile moves in the crack growth direction. At that point the tractions in the integration points and the crack growth rate are the same as for the constant amplitude at that crack length.

The path inside the cohesive law of a single integration point throughout the block loading simulation is compared to the constant amplitude simulations in figure 4.12. During the transition both the base and bridge elements experience secant unloading. Since the layers share nodes, the difference in displacement jump between the start and the end of the transition is the same for the base and bridge layer. If the base layer is already fully damaged at the start of the transition, the integration point can only return to the cohesive law with secant loading, since no fatigue damage development is allowed in the bridge layer. This process of secant reloading after the load transition is shown in figure 4.12a. Figure 4.12b shows that at locations where the base layer is not fully damaged the integration points move gradually to the path of the low constant amplitude test.

On global level, the high-to-low block loading test shows a higher crack growth rate with respect

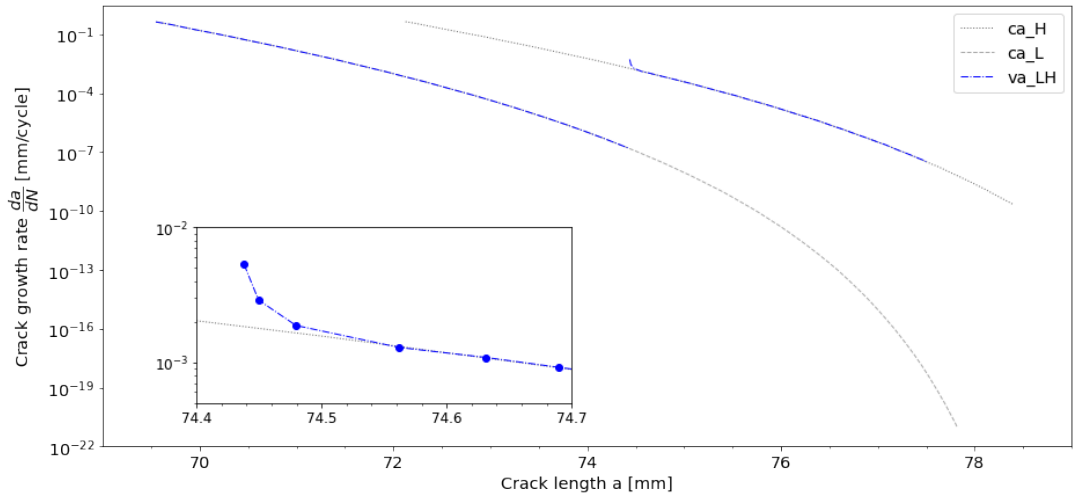

(a) Low-to-high block loading

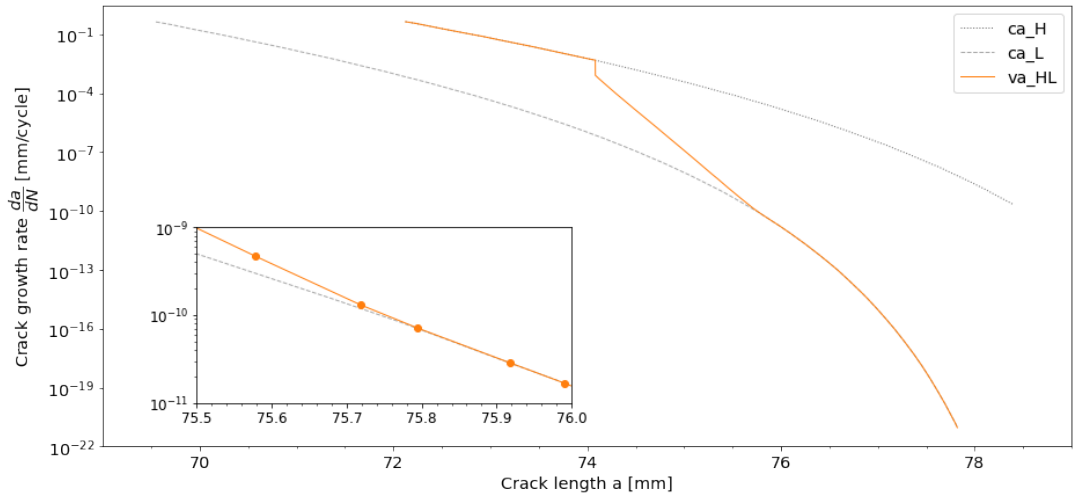

(b) High-to-low block loading

Figure 4.13: Crack growth rate and crack length of load case 2 for the model without fatigue damage in the bridge layer

to the constant amplitude test for approximately $2.5e9$ cycles and a crack extension of 1.7 mm (figure 4.13b). After that it follows the constant amplitude test. This behaviour is not in line with the retardation seen in experiments.

4.4. Effect of fatigue damage accumulation rate in the bridge layer

When the fatigue damage accumulation in the base and bridge layer is the same, as in section 4.2, no load sequence effect is seen. In this section the effect of another fatigue damage accumulation in the bridge layer is examined.

The fatigue damage accumulation is determined by the coefficients β and γ in the fatigue damage rate function (equation 3.1). These coefficients are related to a S-N curve, which is based on the endurance limit and consequently the R-ratio of the applied load. In the previous sections it is implicitly assumed that the ratio between the minimum and maximum displacement of a load block is the same for the base and bridge layer, and that it is the same as the R-ratio of the applied load at the support. In reality the R-ratio experienced by the bridging fibres may not be the same as the R-ratio at the crack tip. For example, Khan et al. (2014) showed that crack closure can increase the effective stress ratio at the crack tip.

To test the effect of other damage accumulation in the base and bridge layer, the coefficients β and γ of the base layer are kept constant and corresponds to the R-ratio $R_{Base} = 0.1$. The corresponding R-ratio of the bridge layer is set to $R_{Br} = 0.5$ or $R_{Br} = -1$. The endurance limit based on the Goodman diagram is smaller for lower of more negative R-ratios. Consequently the S-N curve used to determine the β and γ is steeper. Therefore $R = 0.5$ represents slower fatigue damage accumulation and $R = -1$ represents faster fatigue damage accumulation.

The crack growth rate of the low constant amplitude test for different R-ratios of the bridge layer is shown in figure 4.14. For all R-ratios the crack growth rate follows a straight line on log-scale, which is in line with experiments. At the same crack length the crack growth rate is larger for a smaller R-ratio, since the damage and consequently the stiffness reduction increases faster. Therefore less load cycles are needed to obtain a certain crack length.

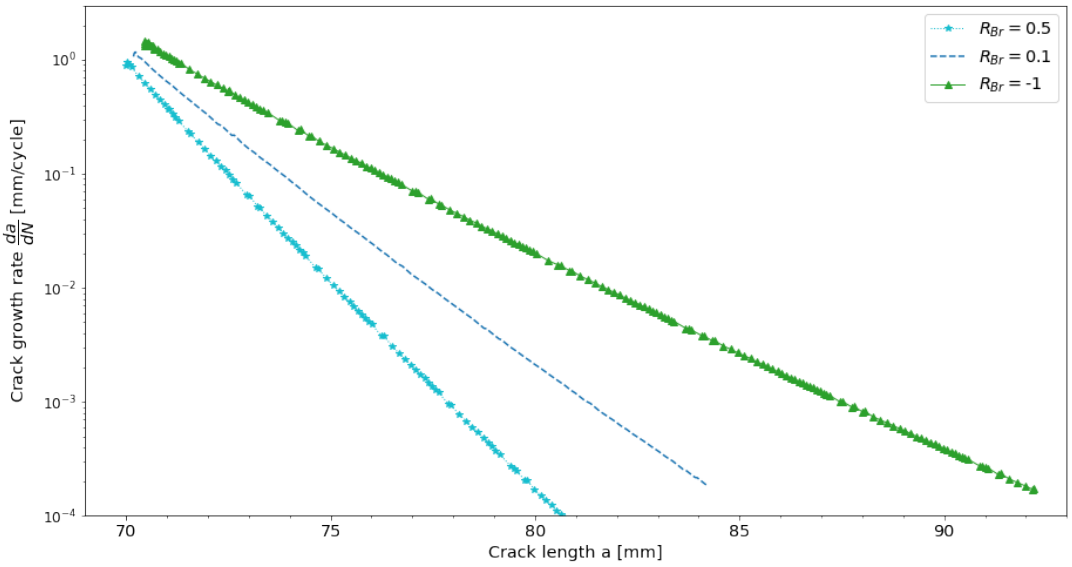

Figure 4.14: Crack growth rate and crack length for ca_L of load case 2 for different R-ratios in the bridge layer

In figure 4.15 the crack growth rate of the block loading is shown for $R_{Br} = 0.5$. When the damage accumulation in the bridge layer is slower than that of the base layer, the low-to-high block loading test shows a lower crack growth rate at the start of the second load block compared to the constant amplitude test. After approximately 80 cycles and a crack extension of 0.4 mm the crack growth rate is the same as the constant amplitude test. The high-to-low block loading test shows a higher crack growth rate for approximately 720 cycles and a crack extension of 0.65 mm, after which it is the same as the constant amplitude test. Although a larger R-ratio for the bridge layer compared to the base layer does give a load history effect, the transition behaviour is the opposite of what is seen in experiments.

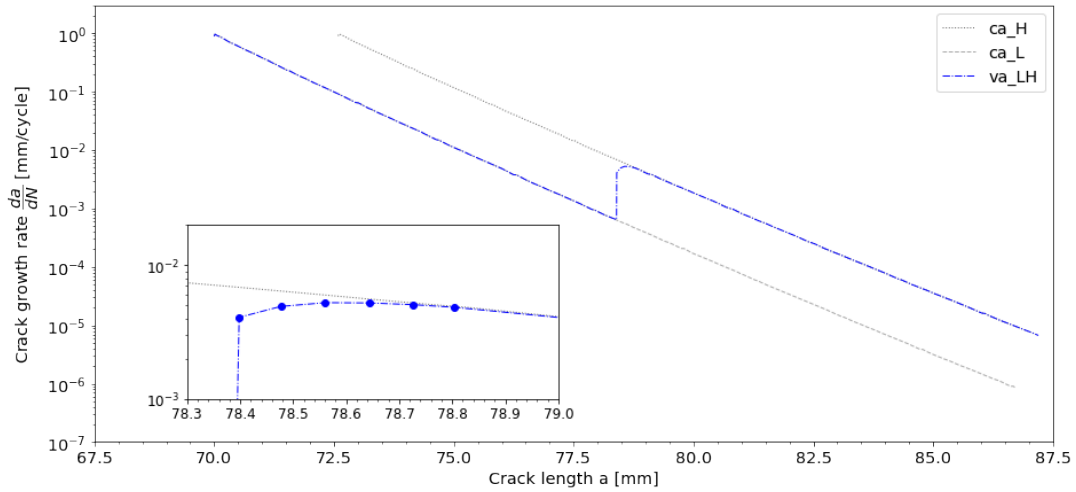

(a) Low-to-high block loading

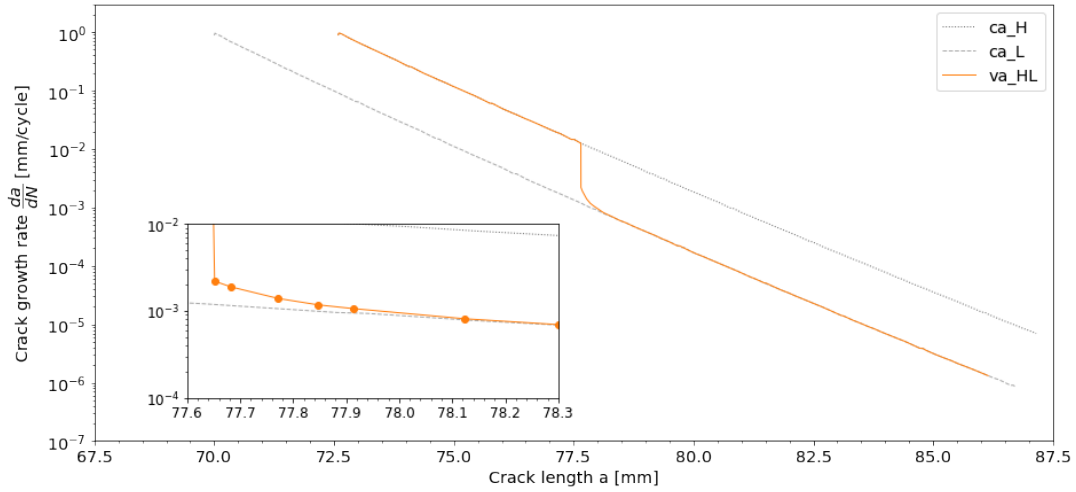

(b) High-to-low block loading

Figure 4.15: Crack growth rate and crack length of load case 2 when $R_{Br} = 0.5$

The transition behaviour when the damage accumulation in the bridge layer is faster than the base layer follows the trend seen in experiments (figure 4.16). The low-to-high transition has a small acceleration for approximately 85 cycles and a crack extension of 0.6 mm and the high-to-low block loading test has a small retardation for approximately 115 cycles and a crack extension of 0.65 mm. The acceleration and retardation for respectively the low-to-high and high-to-low transition are in line with experiments. However, the acceleration and retardation in experiments are more profound and the crack extension over which this behaviour is seen is longer. Furthermore, the crack growth rate directly after the high-to-low transition is slower than the constant amplitude test, instead of first the same and then rapidly decreasing as was seen in the experiments of Jensen et al. (2021b).

The tractions in the block loading test for $R_{Br} = -1$ follow the same trend as seen when the base and bridge layer have the same R-ratio. As the crack progresses, the magnitude of the tractions decrease, while the shape is approximately preserved. During the load transition the tractions decrease or increase without damage accumulation, and during the second load block the crack progresses as usual, namely without changing the traction profile shape.

At the start of the second load block the integration points in the cohesive zone do not have the same location in the cohesive envelope as the constant amplitude test (figure 4.17). For the high-to-low block loading test the displacement jump at the start of the second block is smaller compared to the constant amplitude test, which corresponds to a smaller traction in the base layer and a higher traction in the bridge layer compared to the constant amplitude test. When superimposed the traction is lower,

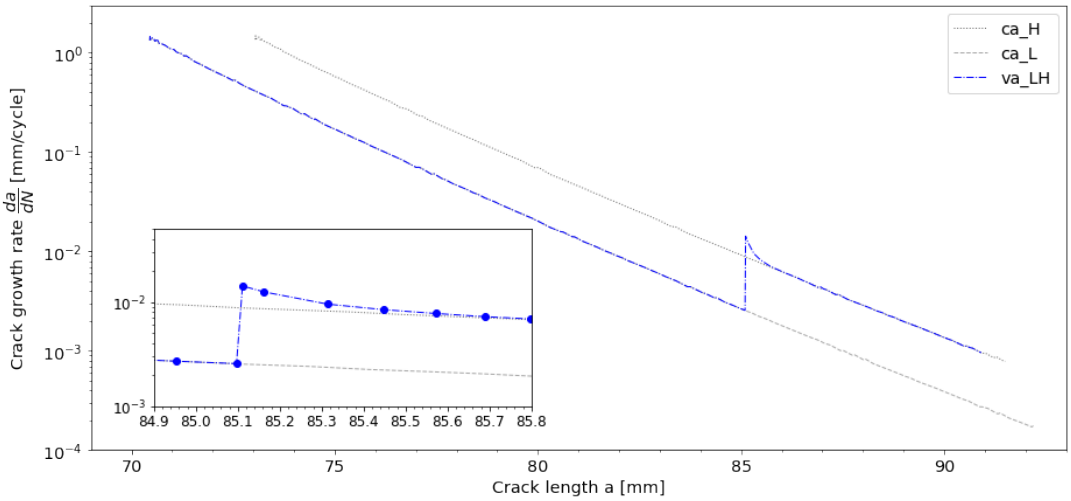

(a) Low-to-high block loading

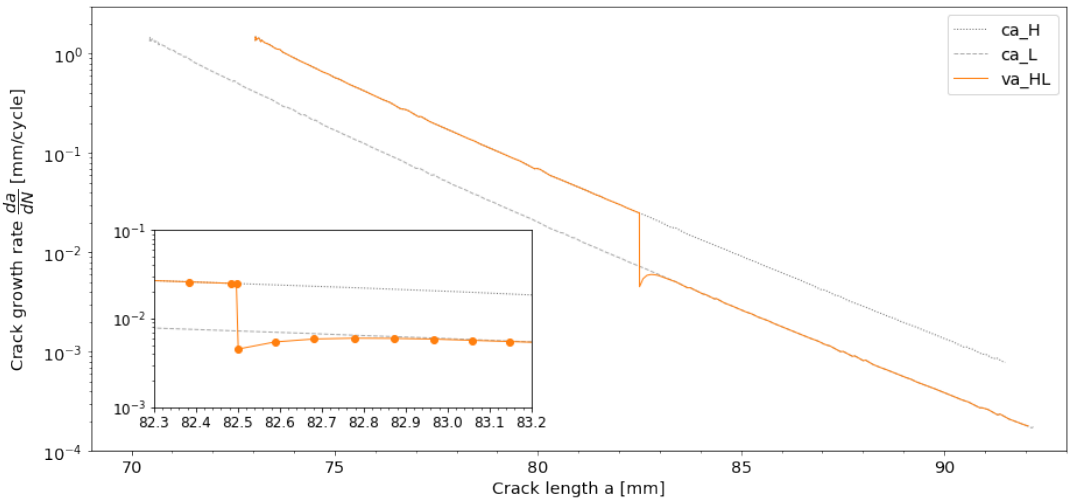

(b) High-to-low block loading

Figure 4.16: Crack growth rate and crack length of load case 2 when R_{Br} = -1

as can be seen in figure 4.17c. For the low-to-high test this is exactly the opposite: the displacement jump and the superposed traction are larger. During the second load block the integration points of both tests accumulate damage, and move gradually and with a slight curve to the constant amplitude line. Once the integration points have the same location in the cohesive envelope as during the constant amplitude test, the crack growth rate of the block loading and the constant amplitude test is the same.

As for the other models, the transition behaviour of the model with different damage accumulation for the base and bridge layer is the same for load case 1 and 2, indicating that the development of the cohesive zone does not influence the results. For load case 3 no load sequence effect is seen, since the quasi-static crack growth during the low-to-high load amplitude transition is larger than the small crack extension over which the transition behaviour is seen in the other load cases.

When the fatigue damage accumulation in the bridge layer is adjusted to correspond to another endurance limit and consequently the R-ratio, both β and γ are changed. The values of the coefficients based on the R-ratio have ranges $13.611 \leq \beta \leq 38.033$ and $0.001911 \leq \gamma \leq 0.002643$, of which the lower values correspond to a lower R-ratio. The transition behaviour seen by changing the coefficients of the bridge layer to the values corresponding to another R-ratio is mainly due to change of β. This becomes clear when the β of the bridge layer is changed while the γ is kept constant, and vice-versa. For all simulations the coefficients of the base layer are $\beta_{base} = 25$ and $\gamma_{base} = 0.002$.

The γ causes a horizontal shift in the crack growth rate curve of the constant amplitude tests. How-

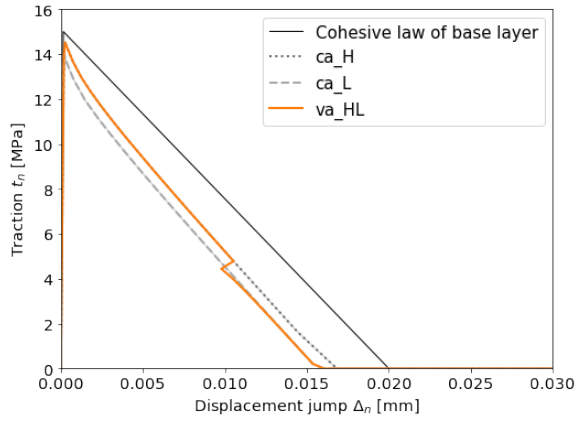

(a) Base layer

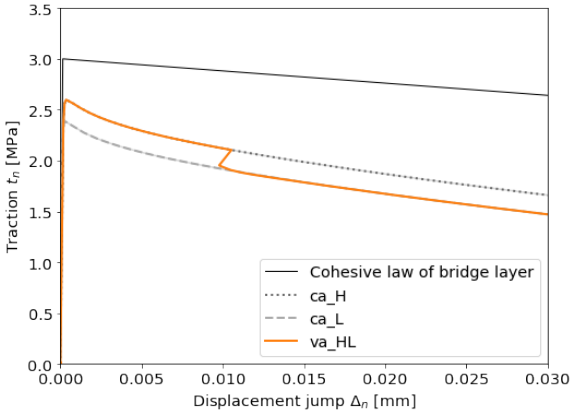

(b) Bridge layer

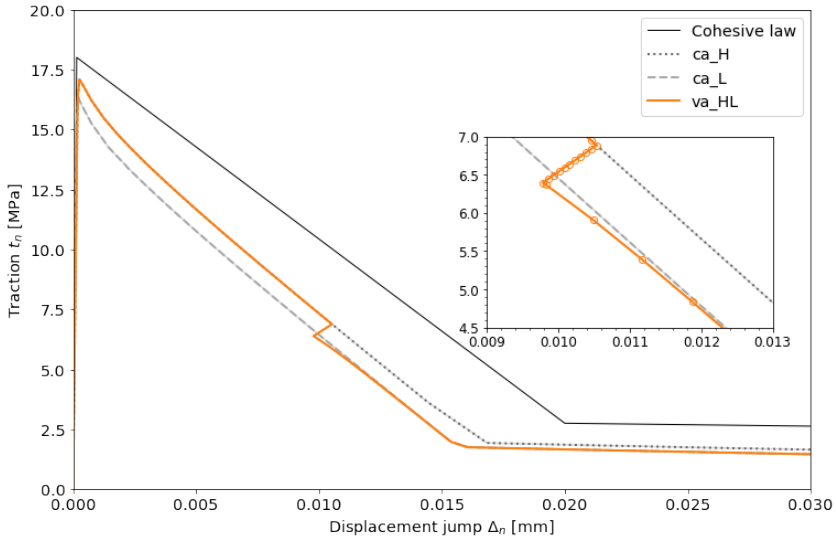

(c) Superposition of the base and bridge layer

Figure 4.17: Traction and displacement jump of element 320 for the high-to-low block loading of load case 2 when R_{Br} = -1

ever, this shift is very small and does not seem to be consistent along the test (figure 4.18). The crack growth rate after the load amplitude change is approximately the same as the constant amplitude test for all values of γ_{Br}. Therefore the contribution of γ to the transition behaviour is small.

The crack growth rate for different values of β_{Br} is shown in figure 4.20. For a larger value of β_{Br} the constant amplitude curve is steeper, indicating a slower fatigue damage accumulation. Since the damage accumulation is not the same for all tests, the crack length and the crack growth rate at the start of the second load block differ. To compare the different simulations, the curves are horizontally and vertically shifted such that the constant amplitude tests intersect at an offset point. A smaller β of the bridge layer than the base layer results in an acceleration after the load amplitude change compared to the constant amplitude test, while a larger β results in a retardation. This behaviour was also observed when comparing $R_{Br} = 0.5$ and $R_{Br} = -1$. The acceleration or retardation is more profound for a larger difference between the β of the base and bridge layer. The crack extension over which the transition behaviour is present is larger for smaller values of β_{Br}.

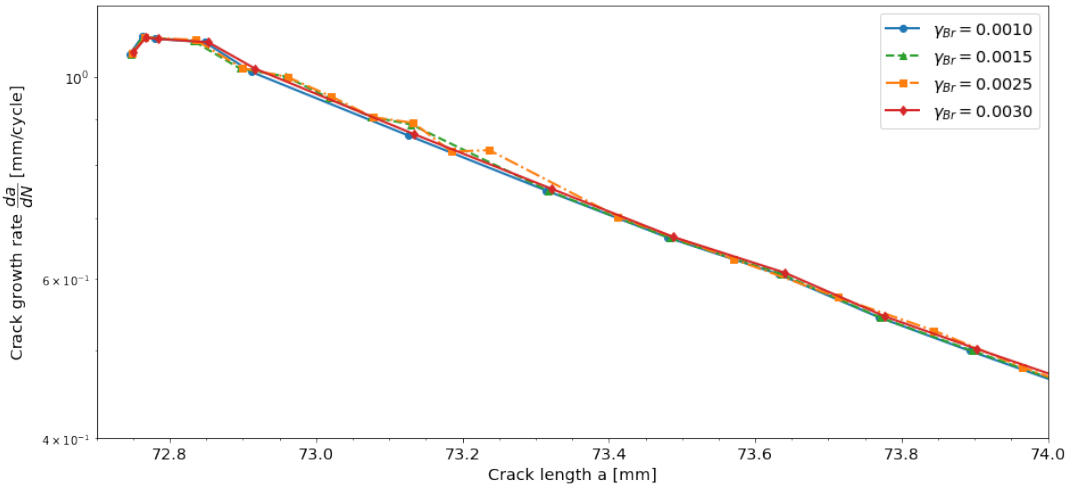

Figure 4.18: Effect of the coefficient γ on crack growth rate for the high constant amplitude test of load case 2

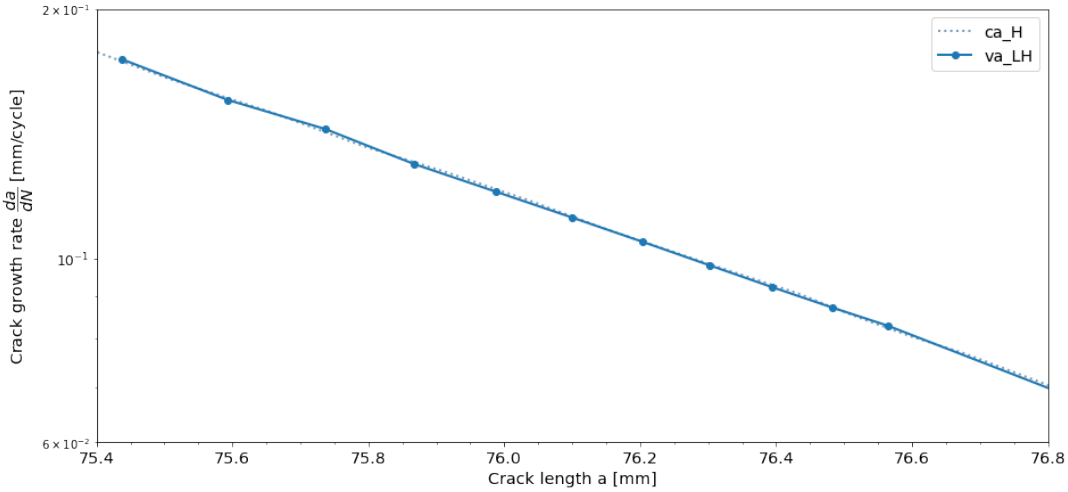

Figure 4.19: Crack growth rate and crack length of load case 2 when $\gamma_{Br} = 0.0010$

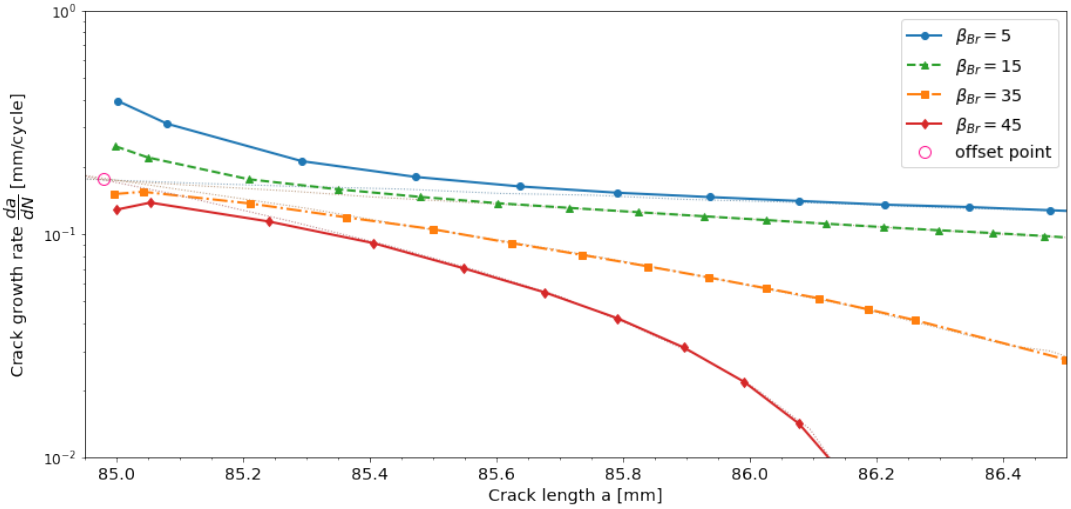

Figure 4.20: Effect of the coefficient β on crack growth rate for the low-to-high block loading test of load case 2. The high constant amplitude tests are shown with a dotted line. The curves are horizontally and vertically shifted such that the constant amplitude tests intersect at the offset point.

5

Conclusion and recommendations

5.1. Conclusion

The fatigue damage model of Dávila (2020) with an implicit fatigue damage update scheme is used to simulate a DCB in mode I constant amplitude loading and block loading. Two element layers with each its own cohesive law is used to take into account the different behaviour of the epoxy and the bridging fibres. The resulting crack growth rate is compared to the trend seen in the experiments done by Jensen et al. (2021b), since the conditions of the simulations are most similar to that of their experiments. According to the experiments a low-to-high load transition will cause a higher crack growth rate after the load transition compared to the high constant amplitude test at the same crack length. With increasing load cycle the crack growth rate decreases until it is the same as the constant amplitude test. After a high-to-low load transition a retardation is seen compared to the low constant amplitude test.

When the base and bridge layer only differ in their quasi-static cohesive law, the conditions at the start of the second load block are the same as for the constant amplitude test at the same crack length, and no load sequence effect is seen. By allowing the bridge layer to only experience quasi-static loading and no fatigue damage accumulation, a history effect is seen. However, for the high-to-low block loading the crack growth rate is larger compared to the constant amplitude test, while experiments indicate a retardation. The acceleration seen after a low-to-high load transition is in line with experiments, although the effect is very small. For both the low-to-high and high-to-low load transition the transition effect decreases as the crack progresses and eventually the same crack growth rate as the constant amplitude is obtained. It should be noted that the crack growth rate development of the constant amplitude tests do not follow the results seen in experiments. Therefore stating that the bridging fibres fail due to quasi-static tearing while the DCB is subjected to a cyclic loading may not be the right failure mechanism.

When the fatigue damage accumulation in the base and bridge layer are different, a load history effect is seen. This difference in fatigue damage accumulation is achieved by adjusting the coefficients of the fatigue damage rate function to the values corresponding to another R-ratio. When the fatigue damage accumulation of the bridge layer is faster than that of the base layer, a higher and lower crack growth rate is seen for the low-to-high and the high-to-low transition respectively. The opposite behaviour is seen when the fatigue damage accumulation in the bridge layer is slower than that of the base layer.

Although the trend for $R_{Br} = -1$ is the same as that seen in experiments, the difference in crack growth rate magnitude and the number of cycles over which the crack growth rate differs from the constant amplitude tests is smaller. Furthermore, the crack growth rate directly after the high-to-low transition is slower than the constant amplitude test, instead of first the same and then rapidly decreasing as was seen in the experiments of Jensen et al. (2021b).

Based on the results of the model with different R-ratios for the base and bridge layer, a possible underlying mechanism for the transition behaviour is that the fatigue damage accumulates faster in the bridging fibres than in the epoxy. Since in the used cohesive fatigue damage model the fatigue damage

rate and the R-ratio are related to each other, one may conclude that the bridging fibres experiencing a larger load difference during a load cycle than the epoxy is a mechanism contributing to the transition behaviour seen in experiments. However, this connection between the R-ratio and the fatigue damage rate is based on several assumptions, mainly through the endurance limit and the S-N curve, and it may be possible that more mechanisms determine the fatigue damage rate function and consequently the transition behaviour.

5.2. Recommendations

In this research a fictitious material is used. As a consequence the results could not exactly be compared to experiments. It may be possible that the used material properties over- or underexaggerate the transition behaviour. To determine whether the cohesive fatigue damage model can accurately model the transition behaviour, the test conditions and material of experiments, for example that of Jensen et al. (2021b), should be simulated.

The transition behaviour seen in experiments with displacement control differ from that with G-control, in which the SERR is constant. For a displacement controlled DCB test it was possible to simulate a load history effect comparable to the trend seen in experiments by altering the coefficients of the fatigue damage rate function. This raises the question whether the same mechanism can also give the transition seen in a DCB test with G-control, which can be modelled with moments at the boundaries.

The fatigue damage rate function used in this research is chosen for its simplicity. Since different damage functions can simulate different failure mechanisms, studying the effect of using another damage function may be interesting. The coefficients of the base and bridge layer can be altered to simulate the different fatigue damage growth in the bridging fibres and the epoxy, but it is also possible to use another fatigue damage function for the bridge layer than for the base layer.

References

Alderliesten, R. C. (2013). Critical review on the assessment of fatigue and fracture in composite materials and structures. *Engineering Failure Analysis*. https://doi.org/10.1016/j.engfailanal.2013.03.022

Bak, B. L. V., Turon, A., Lindgaard, E., & Lund, E. (2017). A benchmark study of simulation methods for high-cycle fatigue-driven delamination based on cohesive zone models. *Composite Structures*, *164*. https://doi.org/10.1016/j.compstruct.2016.11.081

Bender, J. J., Bak, B. L. V., Jensen, S. M., & Lindgaard, E. (2021). Effect of variable amplitude block loading on intralaminar crack initiation and propagation in multidirectional gfrp laminate. *Composites Part B*, *217*. https://doi.org/10.1016/j.compositesb.2021.108905

Blanco, N., Gamstedt, E. K., Asp, L. E., & Costa, J. (2004). Mixed-mode delamination growth in carbon-fibre composite laminates under cyclic loading. *International Journal of Solids and Structures*, *41*. https://doi.org/10.1016/j.ijsolstr.2004.02.040

Dávila, C. G. (2018). A cohesive fatigue model based on the s-n diagram. *Conference paper*. https://doi.org/10.12783/asc33/25992

Dávila, C. G. (2020). From s-n to the paris law with a new mixed-mode cohesive fatigue model for delamination in composites. *Theoretical and Applied Fracture Mechanics*, *106*. https://doi.org/10.1016/j.tafmec.2020.102499

Dávila, C. G., Rose, C. A., & Camanho, P. P. (2009). A procedure for superposing linear cohesive laws to represent multiple damage mechanisms in the fracture of composites. *International Journal of Fracture*, *158*. https://doi.org/10.1007/s10704-009-9366-z

Dávila, C. G., Rose, C. A., Murri, G. B., & Jackson, W. C. (2020). Evaluation of fatigue damage accumulation functions for delamination initiation and propagation. *NASA/TP-2020-220584*.

Gamstedt, E. K., & Sjögren, B. A. (2002). An experimental investigation of the sequence effect in block amplitude loading of cross-ply composite laminates. *International Journal of Fatigue*, *24*. https://doi.org/10.1016/s0142-1123(01)00099-8

Heidari-Rarani, M., Shokrieh, M. M., & Camanho, P. P. (2013). Finite element modeling of mode i delamination growth in laminated dcb specimens with r-curve effects. *Composites: Part B*, *45*. https://doi.org/10.1016/j.compositesb.2012.09.051

Jensen, S. M., Bak, B. L. V., Bender, J. J., & Lindgaard, E. (2021a). Transient delamination growth in gfrp laminates with fibre bridging under variable amplitude loading in g-control. *Composites part B*, *225*. https://doi.org/10.1016/j.compositesb.2021.109296

Jensen, S. M., Bak, B. L. V., Bender, J. J., & Lindgaard, E. (2021b). Transition-behaviour in fatigue-driven delamination of gfrp laminates following step changes in block amplitude loading. *International Journal of Fatigue*, *144*. https://doi.org/10.1016/j.ijfatigue.2020.106045

Jensen, S. M., Carreras, L., Bak, B. L. V., Lequesne, C., & Lindgaard, E. (2023). A crack growth rate model with load history effects for mode i fatigue-driven delamination under multi-level block loading. *International Journal of Fatigue*, *172*. https://doi.org/10.1016/j.ijfatigue.2023.107595

Jensen, S. M., Martos, M. J., Bak, B. L. V., & Lindgaard, E. (2019). Formulation of a mixed-mode multilinear cohesive zone law in an interface finite element for modelling delamination with r-curve effects. *Composite Structures*, *216*. https://doi.org/10.1016/j.compstruct.2019.02.029

Khan, R. (2019). Fiber bridging in composite laminates: A literature review. *Composite Structures*, *229*. https://doi.org/10.1016/j.compstruct.2019.111418

Khan, R., Alderliesten, R., Yao, L., & Benedictus, R. (2014). Crack closure and fibre bridging during delamination growth in carbon fibre/epoxy laminates under mode i fatigue loading. *Composites: Part A*, *67*. https://doi.org/10.1016/j.compositesa.2014.08.028

Latifi, M., van der Meer, F. P., & Sluys, L. J. (2017). Fatigue modeling in composites with the thick level set interface method. *Composites part A*, *101*. https://doi.org/10.1016/j.compositesa.2017.05.035

Pascoe, J. A., Alderliesten, R. C., & Benedictus, R. (2013). Methods for the prediction of fatigue delamination growth in composites and adhesive bonds - a critical review. *Engineering Fracture Mechanics*, *112-113*. https://doi.org/10.1016/j.engfracmech.2013.10.003

Post, N. L., Case, S. W., & Lesko, J. J. (2008). Modeling the variable amplitude fatigue of composite materials: A review and evaluation of the state of the art for spectrum loading. *International Journal of Fatigue*, *30*. https://doi.org/10.1016/j.ijfatigue.2008.07.002

Sarfaraz, R., Vassilopoulos, A. P., & Keller, T. (2013). Block loading fatigue in adhesively bonded pultruded gfrp joints. *International Journal of Fatigue*, *49*. https://doi.org/10.1016/j.ijfatigue.2012.12.006

Stelzer, S., Pinter, G., & Brunner, A. J. (2014). Comparison of quasi-static and cyclic fatigue delamination resistance of carbon fiber reinforced polymer-matrix laminates under different mode loading. *Procedia Materials Science*, *3*. https://doi.org/10.1016/j.mspro.2014.06.177

Turon, A., Costa, J., Camanho, P. P., & Dávila, C. G. (2007). Simulation of delamination in composites under high-cycle fatigue. *Composites part A: applied science and manufacturing*, *38*. https://doi.org/10.1016/j.compositesa.2006.11.009

Yao, L., Alderliesten, R. C., & Benedictus, R. (2015). Interpreting the stress ratio effect on delamination growth in composite laminates using the concept of fatigue fracture toughness. *Composites: Part A*, *78*. https://doi.org/10.1016/j.compositesa.2015.08.005

Yao, L., Alderliesten, R. C., Zhao, M., & Benedictus, R. (2014a). Briding effect on mode i fatigue delamination behavior in composite laminates. *Composites: Part A*, *63*. https://doi.org/10.1016/j.compositesa.2014.04.007

Yao, L., Alderliesten, R. C., Zhao, M., & Benedictus, R. (2014b). Discussion on the use of the strain energy release rate for fatigue delamination characterization. *Composites: Part A*, *66*. https://doi.org/10.1016/j.compositesa.2014.06.018

Yao, L., Sun, Y., Zhao, M., Alderliesten, R. C., & Benedictus, R. (2017). Stress ratio dependence of fibre bridging significance in mode i fatigue delamination growth of composite laminates. *Composites: Part A*, *95*. https://doi.org/10.1016/j.compositesa.2016.11.030

A

Details of the load cases

In this appendix the load cases for all the performed simulations are given. In tables A.1 to A.5 the applied displacement δ_{max} and cumulative number of cycles N_{cum} are given. If a test consists of two load blocks, N_{cum} represents the total number of load cycles the DCB has experienced, thus the number of cycles of first and second load block summed together.

Table A.1: Applied displacement δ_{max} and cumulative number of cycles N_{cum} for the model without bridge layer

Load case		ca_H H	ca_L L	va_HL H	 L	va_LH L	 H
1	δ_{max} [mm]	1.5	1.0	1.5	1.0	1.0	1.5
	N_{cum} [cycle]	1.0e6	1.0e8	2.0e2	1.0e6	5.0e5	1.0e6
2	δ_{max} [mm]	3.5	3.0	3.5	3.0	3.0	3.5
	N_{cum} [cycle]	1.0e4	1.0e4	5.0e1	1.0e4	5.0e1	1.5e3

Table A.2: Applied displacement δ_{max} and cumulative number of cycles N_{cum} for the model with bridge layer

Load case		ca_H H	ca_L L	va_HL H	 L	va_LH L	 H
1	δ_{max} [mm]	3.0	2.5	3.0	2.5	2.5	3.0
	N_{cum} [cycle]	1.0e6	1.0e8	2.0e2	1.0e6	5.0e5	1.0e6
2	δ_{max} [mm]	7.0	6.5	7.0	6.5	6.5	7.0
	N_{cum} [cycle]	1.0e4	1.0e4	5.0e1	1.0e4	5.0e1	1.5e3
3	δ_{max} [mm]	8.0	6.5	8.0	6.5	6.5	8.0
	N_{cum} [cycle]	1.0e4	1.0e4	5.0e1	1.0e4	5.0e1	1.5e3

Table A.3: Applied displacement δ_{max} and cumulative number of cycles N_{cum} for the model without fatigue damage in the bridge layer

Load case		ca_H H	ca_L L	va_HL H	va_HL L	va_LH L	va_LH H
1	δ_{max} [mm]	3.0	2.5	3.0	2.5	2.5	3.0
	N_{cum} [cycle]	1.0e6	1.0e8	2.0e2	1.0e6	5.0e5	1.0e6
2	δ_{max} [mm]	7.0	6.5	7.0	6.5	6.5	7.0
	N_{cum} [cycle]	1.0e9	1.0e20	1.0e2	1.0e20	2.0e6	1.0e7
3	δ_{max} [mm]	8.0	6.5	8.0	6.5	6.5	8.0
	N_{cum} [cycle]	1.0e6	1.0e20	1.0e2	1.0e20	2.0e6	1.0e7

Table A.4: Applied displacement δ_{max} and cumulative number of cycles N_{cum} for the model with $R_{Br} = 0.5$

Load case		ca_H H	ca_L L	va_HL H	va_HL L	va_LH L	va_LH H
2	δ_{max} [mm]	7.0	6.5	7.0	6.5	6.5	7.0
	N_{cum} [cycle]	1.0e6	1.6e6	1.0e2	1.0e6	2.0e3	2.0e5

Table A.5: Applied displacement δ_{max} and cumulative number of cycles N_{cum} for the model with R_{Br} = -1

Load case		ca_H H	ca_L L	va_HL H	va_HL L	va_LH L	va_LH H
1	δ_{max} [mm]	3.0	2.5	3.0	2.5	2.5	3.0
	N_{cum} [cycle]	1.0e6	1.0e8	2.0e3	1.0e6	5.0e5	1.0e6
2	δ_{max} [mm]	7.0	6.5	7.0	6.5	6.5	7.0
	N_{cum} [cycle]	3.5e3	1.6e4	1.0e2	1.5e4	1.0e3	3.5e3
3	δ_{max} [mm]	8.0	6.5	8.0	6.5	6.5	8.0
	N_{cum} [cycle]	5.0e2	1.6e4	2.0e3	1.5e4	1.5e1	1.5e2